ЖЭТФ, 2016, том 150, вып. 1 (7), стр. 69–96 © 2016

STATISTICAL THEORY OF DIFFUSION IN CONCENTRATED BCC AND FCC ALLOYS AND CONCENTRATION DEPENDENCES OF DIFFUSION COEFFICIENTS IN BCC ALLOYS FeCu, FeMn, FeNi, AND FeCr

V. G. Vaks [a], *K. Yu. Khromov* [a,b*], *I. R. Pankratov* [a], *V. V. Popov* [c]

[a] *National Research Center "Kurchatov Institute"*
123182, Moscow, Russia

[b] *Moscow Institute of Physics and Technology (State University)*
117303, Moscow, Russia

[c] *Mikheev Institute of Metal Physics of Ural Branch of Russian Academy of Sciences*
620990, Ekaterinburg, Russia

Received March 31, 2016

The statistical theory of diffusion in concentrated BCC and FCC alloys with arbitrary pairwise interatomic interactions based on the master equation approach is developed. Vacancy-atom correlations are described using both the second-shell-jump and the nearest-neighbor-jump approximations which are shown to be usually sufficiently accurate. General expressions for Onsager coefficients in terms of microscopic interatomic interactions and some statistical averages are given. Both the analytical kinetic mean-field and the Monte Carlo methods for finding these averages are described. The theory developed is used to describe sharp concentration dependences of diffusion coefficients in several iron-based alloy systems. For the BCC alloys FeCu, FeMn, and FeNi, we predict the notable increase of the iron self-diffusion coefficient with solute concentration c, up to several times, even though values of c possible for these alloys do not exceed some percent. For the BCC alloys FeCr at high temperatures $T \gtrsim 1400$ K, we show that the very strong and peculiar concentration dependences of both tracer and chemical diffusion coefficients observed in these alloys can be naturally explained by the theory, without invoking exotic models discussed earlier.

DOI: 10.7868/S0044451016070087

1. INTRODUCTION

Presently, the statistical theory of diffusion has been developed mainly for the dilute alloys [1–5]. Diffusion in concentrated alloys is usually described using various phenomenological models [6, 7], most often the "concentration-dependent Arrhenius" model [8–14] which will be shown below to have no microscopic justification. At the same time, concentration dependences of both intrinsic and tracer diffusion coefficients in alloys are typically very sharp: their variations with concentration reach two–four orders of magnitude [6, 10], and physical understanding of reasons for so strong dependences seems to have both the fundamental and applied interest.

Early theoretical studies of diffusion in concentrated alloys discussed mainly simplified models, such as the "random" alloys with no interatomic interactions. Models providing a good description of diffusion in such alloys have been developed by Manning, Moleko et al., and Belova and Murch [15–17]. Some successful generalizations of these models taking into account "thermodynamic" interatomic interactions (but not kinetic and saddle-point interactions discussed below) have also been suggested [18,19]. Kikuchi and coworkers used the Path Probability Method to describe diffusion in many different concentrated alloy systems [20–22]. However, only some simple models have been considered, and difficulties of generalizations to more consistent and general studies have been noted [22].

* E-mail: khromov_ky@nrcki.ru

The recently-suggested master equation approach [23–30] opens opportunities for microscopic treatments of diffusion in alloys at any composition. This approach enables us to express all Onsager and diffusion coefficients via some statistical averages and microscopic interatomic interactions. These interactions can be calculated employing *ab initio* methods, while statistical averages can be evaluated using various methods of statistical physics. As the level of reliability of both *ab initio* calculations [3–5, 31, 32] and statistical methods [33–35] is steadily increasing, this approach seems to provide a basis for developments of microscopic theories of diffusion in alloys of any composition.

First applications of the master equation approach to studies of diffusion in concentrated alloys have been made by Nastar with coworkers [24–26] (who call this approach "the self-consistent mean-field method"). However, as discussed in Refs. [29] and [30], these studies considered mainly some qualitative or methodical problems, and no discussions of applications to real alloys have been given.

The detailed statistical theory of the steady-state diffusion in concentrated alloys based on the master equation approach has been developed in Refs. [29] and [30]. To be definite, we considered intrinsic and tracer diffusion in FCC substitution alloys with the pairwise nearest-neighbor interactions; for dilute binary alloys it corresponds to the well-known five-frequency model [1, 2]. We derived general expressions for Onsager coefficients in terms of some statistical averages and discussed methods of approximate calculations of these averages. Our simplest statistical approximation, called the "kinetic mean-field approximation" (KMFA), corresponds to using the mean-field approximation for calculations of statistical averages and the pair-cluster approximation — PCA (equivalent to the pair cluster variation method [34]) for calculations of chemical potentials; for dilute alloys, both KMFA and PCA are exact. We also used Monte Carlo methods to find statistical averages. To describe vacancy correlations, we used the nearest-neighbor-jump approximation (NNJA) and the second-shell-jump approximation (SSJA) which generalize analogous methods suggested for dilute binary alloys to the concentrated and multicomponent alloys.

In Ref. [30], we also applied the theory developed to description concentration dependences of diffusion coefficients in alloys CuNi, CuZn, and AgCd for which detailed experimental data about both tracer and intrinsic diffusion are available [6], while the pairwise nearest-neighbor interaction model used in [29, 30] appears to be basically applicable. We found that all main features of strong and peculiar concentration dependences of diffusion coefficients observed in these three alloy systems can be naturally described by the theory, while signs and scales of kinetic and saddle-point interactions found in these estimates agree well with simple physical considerations. The physical reasons for sharp concentration dependences of diffusion coefficients typical of real alloys have also been explained.

The present work aims at two tasks. First, we aim to present the more general and realistic version of the theory which describes not only the simple model of FCC alloys with the nearest-neighbor interatomic interactions used in [29, 30], but both BCC and FCC alloys with arbitrary pairwise interactions. We also describe many refinements of previous methods, including the generalizations of SSJA and KMFA needed to treat these realistic alloy models, as well as the Monte Carlo methods (used earlier [30] with no detailed description).

Second, we use the theory developed to discuss concentration dependences of diffusion coefficients in several alloy systems for which these dependences are very sharp. Here, we first consider the BCC alloys FeCu, FeMn, and FeNi for which diffusion is intensely discussed in connection with applications in nuclear engineering [3–5]. Using available *ab initio* estimates of kinetic and saddle-point interactions for these alloys [5], we predict the notable increase of the iron self-diffusion coefficient with the solute concentration c, up to 2–4 times, even though the solubility limits c_s in these alloys are very low: $c_s \lesssim (0.01–0.04)$. These results imply, in particular, that usual treatments of diffusion in these alloys employing dilute alloy methods [3–5] can lead to notable inaccuracies.

Then, we discuss very sharp concentration dependences of both chemical and tracer diffusion coefficients observed in the BCC alloys FeCr at high temperatures $T \gtrsim 1400$ K. With increasing the chromium concentration c, these coefficients decrease by about four orders of magnitude, which is one of the most strong variations of diffusion coefficients with composition known for alloys [10]. These sharp dependences were discussed by many authors [8–14],mainly in terms of the above-mentioned "concentration-dependent Arrhenius" model. It yields unusual concentration anomalies in parameters of this model at $c \sim 0.6$, and some exotic models to explain these anomalies have been suggested [10, 11]. We use the available data [8–14, 37] and theoretical calculations [5] to estimate interatomic interactions important for diffusion in these alloys. We show that all strong concentration dependences of diffusion coefficients mentioned above can be naturally described by the statistical theory, while the anomalies discussed

in Refs. [10, 11] are related just to the inadequacy of the concentration-dependent Arrhenius model for description of concentration dependences of diffusion coefficients.

The paper is organized as follows. In Sec. 2, we present main relations from papers [29, 30] needed for what follows. In Sec. 3, we derive expressions for correlation operators $\hat{b}^p$ which describe influence of neighboring solute atoms on the probability of a vacancy-atom exchange for both BCC and FCC alloys with arbitrary pairwise interactions. In Sec. 4, we discuss approximations for description of vacancy correlations, NNJA and SSJA, and expressions for coefficients in basic equations (17) and (19) for atomic fluxes and for the fields describing vacancy correlations via certain statistical averages. In Sec. 5, we describe methods of calculations of these averages in the kinetic mean-field approximation (KMFA) which generalize those used earlier [29, 30] to the case of arbitrary pairwise interactions in BCC and FCC alloys. In Sec. 6, we discuss Monte Carlo methods of evaluation of statistical averages which enable us to find these averages (for the given interaction model) practically exactly. In Sec. 7, we present SSJA and NNJA expressions for correlation factors in dilute BCC and FCC alloys (which generalize the earlier results [1, 2] to the case of arbitrary interactions), and also for the tracer correlation factors in BCC random alloys for which comparison with the Monte Carlo results [17] enables us to estimate accuracy of SSJA and NNJA. In Secs. 8 and 9, we discuss applications of the statistical theory developed to the description of strong concentration dependences of diffusion coefficients in BCC alloys FeCu, FeMn, FeNi, and FeCu mentioned above. Our main conclusions are summarized in Sec. 10.

2. STATISTICAL EXPRESSION FOR ONSAGER AND DIFFUSION COEFFICIENTS IN A SUBSTITUTION ALLOY

In this section, we present main relations of theory developed in Refs. [29, 30] needed for what follows. We consider a substitution alloy with $(m+1)$ components p' including host atoms denoted as h, solute atoms denoted by letters α, β, λ, and vacancies denoted as v. Latin letters p and q denote all kinds of atoms, h and α, while Greek letters ρ, σ, τ denote solute atoms α and vacancies v. Various distributions of atoms over lattice sites i are described by the different occupation number sets $\{n_i^{p'}\}$ where $n_i^{p'}$ is 1 when site i is occupied by a p'-species component, and 0 otherwise. For each site i, operators $n_i^{p'}$ obey the identity $\sum_{p'} n_i^{p'} = 1$, and we eliminate operators n_i^h for host atoms putting $n_i^h = 1 - \sum_\rho n_i^\rho$.

We use the pairwise interaction model for which the total configurational Hamiltonian H^t can be expressed via n_i^p and n_i^v and couplings V_{ij}^{pq} and V_{ij}^{pv} as follows:

$$H^t = \sum_{i>j} \sum_{pq} V_{ij}^{pq} n_i^p n_j^q + \sum_{ij} \sum_{p} V_{ij}^{pv} n_i^p n_j^v, \quad (1)$$

where we neglect terms with interaction of vacancies as their fractional concentration (to be called simply "concentration") $c_v = \langle n_i^v \rangle$ is very low: $c_v \ll c_p = \langle n_i^p \rangle$. After elimination of operators n_i^h, the interaction Hamiltonian H_{int} takes the form

$$H_{int} = \sum_{\alpha\beta, i>j} v_{ij}^{\alpha\beta} n_i^\alpha n_j^\beta + \sum_{\alpha, ij} v_{ij}^{\alpha v} n_i^\alpha n_j^v, \quad (2)$$

where interactions $v_{ij}^{\alpha\beta}$ and $v_{ij}^{\alpha v}$ are linearly expressed via V_{ij}^{pq} and V_{ij}^{pv} in Eq. (1).

The fundamental master equation for the probability P of finding an occupation number set $\{n_i^\rho\} = \xi$ can be written as [23]:

$$\frac{dP(\xi)}{dt} = \sum_\eta [W(\xi,\eta)P(\eta) - W(\eta,\xi)P(\xi)] \equiv \hat{S}P, \quad (3)$$

where $W(\xi,\eta)$ is the $\eta \to \xi$ transition probability per unit time, and the transfer matrix $\hat{S}$ is the sum of probabilities W_{ij}^{pv} of inter-site atomic exchanges ("jumps") $pi \leftrightharpoons vj$ between neighboring sites i and j per unit time:

$$\begin{aligned} W_{ij}^{pv} &= n_i^p n_j^v \omega_{pv}^{eff} \exp[-\beta(\hat{E}_{pi,vj}^{SP} - \hat{E}_{pi,vj}^{in})], \\ \hat{E}_{pi,vj}^{SP} &= E_h^p + \sum_{\lambda l} \Delta_{p,ij}^{\lambda l} n_l^\lambda. \end{aligned} \quad (4)$$

Here, ω_{pv}^{eff} is the effective attempt frequency for a jumping atom p, $\beta = 1/T$ is the reciprocal temperature, $\hat{E}_{pi,vj}^{in}$ is the initial (before the jump) configurational energy of a jumping atom p and a vacancy, $\hat{E}_{pi,vj}^{SP}$ is the saddle-point energy, and terms $\Delta_{p,ij}^{\lambda l}$ describing dependences of the saddle-point energy $\hat{E}_{pi,vj}^{SP}$ on atomic configurations near bond (i,j) are called the "saddle-point interactions". The probability P in (3) can be written as [23, 24]

$$P\{n_i^\rho\} = \exp\left[\beta\Big(\Omega + \sum_{\rho i} \lambda_i^\rho n_i^\rho - H_{int} - \hat{h}_{eff}\Big)\right], \quad (5)$$

$$\hat{h}_{eff} = \frac{1}{2} \sum_{\rho\sigma, ij} h_{ij}^{\rho\sigma} n_i^\rho n_j^\sigma + \frac{1}{6} \sum_{\rho\sigma\tau, ijk} h_{ijk}^{\rho\sigma\tau} n_i^\rho n_j^\sigma n_k^\tau + \ldots \quad (6)$$

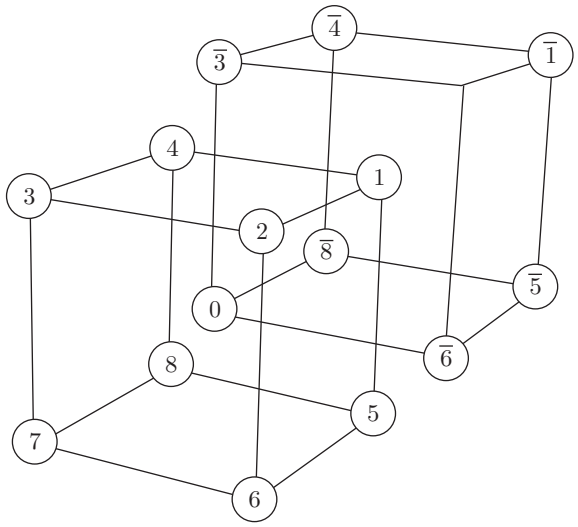

Fig. 1. Bond (0,1) in the BCC lattice and its nearest neighbors, sites k and $\bar{k}$ discussed in the text

Here, $\lambda_i^\rho = \mu_i^\rho - \mu_i^h$ are "site chemical potentials" for solute atoms or vacancies with respect to host atoms and constant Ω is determined by normalization. The operator $\hat{h}_{eff}$ (6) and "effective interactions" $h_{ij\ldots}^{\rho\sigma\ldots}$ (to be also called "fields" for brevity) describe changes in the stationary distribution of vacancies with respect to different species atoms due to the steady-sate diffusion, or vacancy correlations. The first term in (6) describes pairwise vacancy correlations, while the second and the rest terms, the non-pairwise ones. Below, we consider only the first term in (6) as the non-pairwise vacancy correlations seem to be usually insignificant [30].

Multiplying Eq. (3) by operators n_i^p and $n_i^\alpha n_j^p$ and summing over all configurations $\{n_j^\lambda\}$, we obtain equations which determine evolution of "local concentrations" $c_i^p = \langle n_i^p \rangle$ and evolution of two-site averages $\langle n_i^\alpha n_j^p \rangle$:

$$\frac{dc_i^p}{dt} = \langle n_i^p \hat{S} \rangle, \quad \frac{d}{dt}\langle n_i^\alpha n_j^p \rangle = \langle n_i^\alpha n_j^p \hat{S} \rangle \tag{7}$$

where $\langle \ldots \rangle$ means averaging over distribution (5).

The steady-state diffusion under consideration corresponds to the stationary distribution for which the right-hand sides of Eqs. (7) vanish. Such diffusion is commonly described in terms of Onsager coefficients L_{pq} which relate the atomic flux density $\mathbf{J}_p$ to the chemical potential gradients $\nabla\mu_q$ supposed to be small and constant. For a cubic crystal, Onsager relations have the form [2]

$$\mathbf{J}_p = -\sum_q L_{pq} \nabla \mu_q. \tag{8}$$

Microscopic expressions for Onsager coefficients L_{pq} in (8) are obtained using the microscopic expression for flux density $\mathbf{J}_p$ which can be derived from Eqs. (3)–(7). For the steady-state diffusion, differences of local chemical potentials, $\mu_j^q - \mu_i^q = \delta\mu_q$ which enter into Eqs. (7) are proportional to gradients $\nabla\mu_q$ in (8) being small and constant, while fields $h_{ij}^{\alpha\rho}$ in (6) are proportional to these differences. Linearizing Eqs. (7) in $\delta\mu_q$ and $h_{ij}^{\alpha\rho}$, we obtain the linear equations which relate the atomic flux J_{ij}^p through each bond (ij), e. g. bond (0,1) shown in Fig. 1, to the chemical potential difference $\delta\mu_p$ and fields $h_{ij}^{\alpha\rho}$:

$$J_{0\to1}^p = -\beta \left[\langle w_p \rangle (\delta\mu_p + 2h_1^{pv}) - \right.$$
$$\left. - \sum_{\lambda i} \nu_{pi}^\lambda (h_{0i}^{v\lambda} - h_{1i}^{v\lambda} - h_{0i}^{p\lambda} + h_{1i}^{p\lambda}) \right], \tag{9}$$

where $\delta\mu_p$ is $\mu_1^p - \mu_0^p$ and h_1^{pv} is the nearest-neighbor effective interaction. Symbol $\langle \ldots \rangle$ in Eq. (9) and below means statistical averaging over equilibrium Gibbs distribution given by Eq. (5) with constant values of chemical potentials $\lambda_i^\rho = \lambda_\rho$ and $\hat{h}_{eff} = 0$. The operator $\hat{w}_{01}^p$ describes the probability of a jump $p0 \rightleftharpoons v1$. It has the form of a product of the constant Γ_p and the "correlation" operator $\hat{b}_{01}^p$:

$$\hat{w}_{01}^p = \Gamma_p \hat{b}_{01}^p, \tag{10}$$

$$\Gamma_\alpha = \frac{\omega_{\alpha 0} c_\alpha a_\alpha}{c_h^2}, \quad \Gamma_h = \frac{\omega_{h0}}{c_h}. \tag{11}$$

Here, ω_{p0} is the mean frequency of $pi \rightleftharpoons vj$ jumps for a p-species atom in a pure host metal. It is expressed via the vacancy concentration c_{v0} in this metal, the effective attempt frequency ω_{pv}^{eff} in Eq. (4), and the activation energy E_{ac}^{pv} for a $p \rightleftharpoons v$ jump as follows:

$$\omega_{p0} = c_{v0} \omega_{pv}^{eff} \exp(-\beta E_{ac}^{pv}). \tag{12}$$

Factor a_α (11) is the reduced thermodynamic activity coefficient for α-species atoms; for a binary alloy, its form is illustrated by Eq. (53) below.

Factor $\hat{b}_{01}^p$ in Eq. (10) is the "correlation operator" which describes influence of presence of solute atoms near the bond $(0,1)$ on the $p0 \rightleftharpoons v1$ jump probability:

$$\hat{b}_{ij}^p = n_i^h n_j^h \times$$
$$\times \exp\left[\sum_{\alpha l} \beta (u_{il}^\alpha + u_{jl}^\alpha) n_l^\alpha - \sum_{\alpha l} \beta \Delta_{p,ij}^{\alpha l} n_l^\alpha \right]. \tag{13}$$

Here, $\Delta^{\alpha l}_{p,ij}$ is the same as in Eq. (4), while the parameters u^{α}_{il} called "kinetic interactions" are expressed via couplings V^{pq}_{ij} in Eq. (1) as follows:

$$u^{\alpha}_{il} = V^{h\alpha}_{il} - V^{hh}_{il}. \tag{14}$$

The average $\langle \hat{w}^p_{01} \rangle$ in (10) can be expressed via the mean frequency ω_p of $p \rightleftharpoons v$ jumps for a p-species atom:

$$\langle \hat{w}^p_{01} \rangle = c_p\, \omega_p, \tag{15}$$

where $c_p = \langle n^p_i \rangle$ is the mean concentration. Below, we usually employ frequencies ω_p rather than averages $\langle w_p \rangle$ as these frequencies have a more clear physical meaning.

Fields $h^{\alpha\rho}_{ij}$ in Eqs. (9) are found from the condition of vanishing of the right-hand side of the second equation (7) [24, 29]. It yields the following equations for $h^{\alpha\rho}_{ij}$:

$$\sum_{k\neq 0\neq j} \Bigg[m^{pj}_{\alpha,0k} \left(\delta\mu^{\alpha}_{k0} + 2h^{\alpha v}_{0k}\right) - \\ - \sum_{\lambda l} t^{pj,\lambda l}_{\alpha,0k} \left(h^{v\lambda}_{0l} - h^{v\lambda}_{kl} - h^{\alpha\lambda}_{0l} + h^{\alpha\lambda}_{kl}\right) + \\ + m^{\alpha 0}_{p,jk} (\delta\mu^{p}_{kj} + 2h^{pv}_{jk}) - \\ - \sum_{\lambda l} t^{\alpha 0,\lambda l}_{h,jk} \left(h^{v\lambda}_{jl} - h^{v\lambda}_{kl} - h^{p\lambda}_{jl} + h^{p\lambda}_{kl}\right) \Bigg] = 0, \tag{16}$$

where $m^{qj}_{p,ik}$ is $\langle \hat{w}^p_{ik} n^q_j \rangle$ and $t^{qj,\lambda l}_{p,ik}$ is $\langle \hat{w}^p_{ik} n^q_j n^{\lambda}_l \rangle$.

For both BCC and FCC alloys, we consider diffusion along the crystal axis z when reduced chemical potentials $\mu^p_i = \mu^p(\mathbf{R}_i)$ depend only on z_i. For the BCC alloy, we denote positions of sites 0 and 1 in Eqs. (9) as $\mathbf{R}_0 = (0,0,0)$ and $\mathbf{R}_1 = (a_0/2, a_0/2, a_0/2)$, where a_0 is the BCC lattice constant, while sites near the bond $(0,1)$ are numbered as shown in Fig. 1. In this Figure, sites with positions $\mathbf{R}_k$ for k between 1 and 8 correspond to the nearest neighbors of site "0" positioned at $\mathbf{R}_0 = 0$, while sites positioned at $\mathbf{R}_{\bar{k}} \equiv \mathbf{R}_{k,1} = \mathbf{R}_k + \mathbf{R}_1$ correspond to the nearest neighbors of site "1" with $\mathbf{R}_1 = (a_0/2, a_0/2, a_0/2)$. For the FCC alloy, we denote positions of sites 0 and 1 in Eqs. (9) as $\mathbf{R}_0 = (0,0,0)$ and $\mathbf{R}_1 = (0, a_0/2, a_0/2)$, where a_0 is the FCC lattice constant, while sites near the bond $(0,1)$ are numbered as shown in Fig. 2. Quantity $\delta\mu_p$ in Eqs. (9) is the chemical potential difference between neighboring atomic planes along z axis: $\delta\mu_p = \mu_p(a_0/2) - \mu_p(0)$. The field $h^{\rho\lambda}_{0l} = h^{\rho\lambda}(\mathbf{R}_{0l})$ does not change under rotations of vector $\mathbf{R}_{0l} = (x_{0l}, y_{0l}, z_{0l})$ around z-axis, and it changes sign under reflection with respect to xy plane: $h^{\rho\lambda}(x_{0l}, y_{0l}, -z_{0l}) = -h^{\rho\lambda}(x_{0l}, y_{0l}, z_{0l})$. For brevity, we

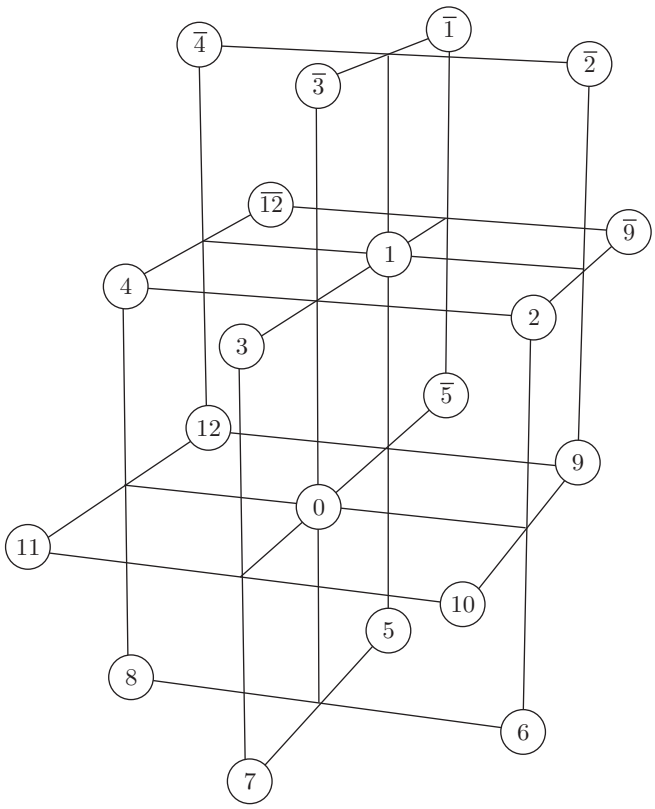

Fig. 2. Bond (0,1) in the FCC lattice and its nearest neighbors, sites k and $\bar{k}$ discussed in the text

denote the set of crystallographically equivalent sites with the same positive value $z_{0l_n} = z^+_{l_n} > 0$ as l^+_n, the similar set with the negative value $z_{0l_n} = -z^+_{l_n}$, as l^-_n, and fields $h^{\rho\lambda}(\mathbf{R}_{l^+_n})$ or $h^{\rho\lambda}(\mathbf{R}_{l^-_n})$ corresponding to the set of sites l^+_n or l^-_n, as $h^{\rho\lambda}_n$ or $(-h^{\rho\lambda}_n)$. Index n which numbers different sets of equivalent sites, l^+_n and l^-_n, is supposed to increase with the distance $|\mathbf{R}_{0l}|$, and for a given $|\mathbf{R}_{0l}|$, it increases with the z_{0l} value. Thus, $n = 1$ corresponds to the nearest-neighbor field $h^{\rho\lambda}_1 = h^{\rho\lambda}(\mathbf{R}_{01})$, and Eqs. (9) can be concisely written as

$$J^p_{0\to 1} = -\beta \Bigg[c_p \omega_p (\delta\mu_p + 2h^{pv}_1) + \\ + \sum_{\lambda} \sum_{n=1}^{n_{max}} l^{\lambda}_{p,n} (h^{\lambda v}_n - h^{\lambda p}_n) \Bigg]. \tag{17}$$

Here, n_{max} is the total number of non-equivalent fields $h^{\rho\lambda}_n$ considered, and the higher n_{max} correspond to taking into account the more distant vacancy correlation effects [24]. Coefficients $l^{\lambda}_{p,n}$ in Eq. (17) are defined as follows:

$$l^{\lambda}_{p,n} = \sum_{l^+_n,\, l^-_n} \langle \hat{w}^p_{01}(n_{l^+_n} - n_{l^-_n} - n_{1,l^+_n} + n_{1,l^-_n})^{\lambda}\rangle. \quad (18)$$

Here, $n_{l^{\pm}_n} = n(\mathbf{R}_{l^{\pm}_n})$, $n_{1,l^{\pm}_n} = n(\mathbf{R}_{l^{\pm}_n} + \mathbf{R}_1)$, and index λ at brackets means that it should be put at each term within brackets, e. g. $(n_{l^+_n} + \ldots)^{\lambda} = (n^{\lambda}_{l^+_n} + \ldots)$.

Using the same notation as in Eq. (17), we can concisely write Eqs. (16) as

$$m^p_{\alpha,n}(\delta\mu_\alpha + 2h^{\alpha v}_1) - m^{\alpha}_{p,n}(\delta\mu_p + 2h^{pv}_1) - \\ + \sum_{\lambda}\sum_{m=1}^{n_{max}} \Big[(t^{p\lambda}_{\alpha,nm} - t^{\alpha\lambda}_{p,nm})h^{\lambda v}_m - \\ - t^{p\lambda}_{\alpha,nm}h^{\lambda\alpha}_m + t^{\alpha\lambda}_{p,nm}h^{\lambda p}_m\Big] = 0, \quad (19)$$

where coefficients $t^{q\lambda}_{p,nm}$ and $m^q_{p,n}$ are defined as follows:

$$t^{q\lambda}_{p,nm} = \sum_{k=1}^{k_{max}} \sum_{l^+_m,\, l^-_m} \langle \hat{w}^p_{0k} n^q_{n,1}(n_{l^+_m} - n_{l^-_m} - \\ - n_{k,l^+_m} + n_{k,l^-_m})^{\lambda}\rangle, \quad (20)$$

$$m^q_{p,n} = \sum_{k=1}^{4} \langle (\hat{w}^p_{0k} - \hat{w}^p_{0,k+4}) n^q_{n,1}\rangle\,.$$

Here, $n_{l^+_m}$ and $n_{l^-_m}$ are the same as in (18); operator $n^q_{n,1} = n^q(\mathbf{R}_{n,1})$ corresponds to the vector $\mathbf{R}_{n,1}$ chosen as "the first one" in the set of vectors $\mathbf{R}_{l^+_n}$; k_{max} is the number of nearest neighbors equal to 12 for an FCC alloy and 8 for a BCC alloy; $n_{k,l^{\pm}_n}$ defined similarly to $n_{1,l^{\pm}_n}$ in Eq. (18) is $n(\mathbf{R}_{l^{\pm}_n} + \mathbf{R}_k)$; and we took into account symmetry or antisymmetry of each average in Eq. (19) with respect to reflections $\mathbf{R}_{n,1} \to (-\mathbf{R}_{n,1})$. Note that fields $h^{p\lambda}_n = -h^{\lambda p}_n$ in Eqs. (17) and (20) for $p = h$ should be put zero as they are absent in the operator $\hat{h}_{eff}$ (6).

To solve Eqs. (17) and (19) for the chosen number n_{max} of effective fields describing vacancy correlations, we should calculate coefficients $l^{\lambda}_{p,n}$, $m^q_{p,n}$, and $t^{q\lambda}_{p,nm}$ in these equations. Eqs. (20) for $m^q_{p,n}$ and $t^{q\lambda}_{p,nm}$ (unlike Eqs. (18) for $l^{\lambda}_{p,n}$) include operators $\hat{w}^p_{0k}$ describing the $p \leftrightharpoons v$ exchange along bond $(0,k)$ rather than that along bond (0,1). To reduce these coefficients to the standard form which includes only operator $\hat{w}^p_{01}$, we can use operators of turn, $\hat{T}_k$, which transform bonds $(0,k)$ into bond (0,1). Then, Eqs. (20) can be written as follows:

$$m^q_{p,n} = \left\langle \hat{w}^p_{01} \sum_{k=1}^{4} (\hat{T}_k - \hat{T}_{k+4}) n^q_{n,1} \right\rangle, \\ t^{q\lambda}_{p,nm} = \left\langle \hat{w}^p_{01} \sum_{k=1}^{k_{max}} \hat{T}_k (n^q_{n,1}\sigma^{\lambda}_{k,m}) \right\rangle, \quad (21)$$

$$\sigma^{\lambda}_{k,m} = \sum_{l^+_m,\, l^-_m} (n_{l^+_m} - n_{l^-_m} - n_{k,l^+_m} + n_{k,l^-_m})^{\lambda}\,. \quad (22)$$

Here, action of the operator of turn $\hat{T}_k$ on each occupation operator $n^q_i \equiv n^q(\mathbf{R}_i)$ corresponds to the turn of the vector $\mathbf{R}_i$: $\hat{T}_k n^q_i = n^q(\hat{T}_k\mathbf{R}_i)$. The "turned" vectors $\hat{T}_k\mathbf{R}_i$ for each k and $\mathbf{R}_i$ are determined by Tables A1 or A2 in Appendix 1.

Equations (18), (21), (22) show that coefficients $l^{\lambda}_{p,n}$, $m^q_{p,n}$, and $t^{q\lambda}_{p,nm}$ in Eqs. (17) and (19) are expressed via one-site or two-site statistical averages of the following form:

$$\nu^q_{pi} = \langle \hat{w}^p_{01} n^q_i\rangle, \quad \nu^{q\lambda}_{p,ij} = \langle \hat{w}^p_{01} n^q_i n^{\lambda}_j\rangle\,. \quad (23)$$

Note that due to the first identity (41), terms $t^{q\lambda}_{p,nm}$ in Eq. (22) include not only two-site averages $\nu^{q\lambda}_{p,ij}$ in (23), but also one-site averages ν^q_{pi} which arise when the site $\mathbf{R}_{n,1}$ coincides with $\mathbf{R}_{l^{\pm}_m}$ or $\mathbf{R}_{k,l^{\pm}_m}$. Hence term $t^{q\lambda}_{p,nm}$ (22) can be written as

$$t^{q\lambda}_{p,nm} = \delta_{q\lambda} t^q_{1p,nm} + t^{q\lambda}_{2p,nm}, \quad (24)$$

where the first term includes one-site averages $\nu^q_{p,i}$, while the second one includes "true" two-site averages $\nu^{q\lambda}_{p,ij}$ with $i \neq j$. Explicit expressions for averages (21)–(24) are discussed below.

Equations (19) enable us to express all fields $h^{\alpha\rho}_n$ as linear combinations of $\delta\mu_q$. Then, substitution of these expressions into Eqs. (17) yields linear relations between fluxes $J^p_{0\to 1}$ and differences $\delta\mu_p$:

$$J^p_{0\to 1} = \sum_q A_{pq}\delta\mu_q, \quad (25)$$

where A_{pq} are some functions of coefficients $l^{\lambda}_{p,n}$, $m^q_{p,n}$, and $t^{q\lambda}_{p,n}$ in Eqs. (19). Equations (25) are evidently equivalent to Onsager relations (8). Simple geometrical considerations described in [29] show that for both FCC and BCC alloys, Onsager coefficients L_{pq} are expressed via coefficients A_{pq} in Eq. (25) and the lattice constant a_0 as follows:

$$L_{pq} = -\frac{4A_{pq}}{a_0} = -na_0^2 A_{pq}, \quad (26)$$

where n is the atomic density equal to $4/a_0^3$ for an FCC alloy, or to $2/a_0^3$ for a BCC alloy. Equations (26) enable us to microscopically calculate Onsager coefficients.

Let us now discuss expressions for intrinsic and tracer diffusion coefficients in a BCC or FCC binary alloy AB. As discussed in [29], each intrinsic diffusion coefficient D_p with p equal to A or B can be conveniently written in terms of "correlative" Onsager coefficients L^c_{pq} which describe vacancy correlation effects and are related to the conventional Onsager coefficients L_{pq} in Eq. (8) as follows:

$$\begin{aligned}\frac{T}{na_0^2}\,L_{AA} &= \omega_A c_A(1-cL^c_{AA}),\\ \frac{T}{na_0^2}\,L_{AB} &= \omega_B c c_A L^c_{AB},\\ \frac{T}{na_0^2}\,L_{BB} &= \omega_B c(1-c_A L^c_{BB}).\end{aligned} \tag{27}$$

Here, $c = c_B$, $c_A = 1-c$, and $1/n = \bar{v}$ is the mean volume per atom supposed to obey the Vegard's law:

$$\bar{v} \equiv \frac{1}{n} = c_A\overline{v}_A + c\overline{v}_B, \tag{28}$$

where $\overline{v}_p$ is atomic volume of a p-component in an alloy. Then, each intrinsic diffusion coefficient D_p can be written as follows:

$$\begin{aligned}D_A &= \frac{a_0^2}{n\overline{v}_B}\,\omega_A f_A \Phi,\\ D_B &= \frac{a_0^2}{n\overline{v}_A}\,\omega_B f_B \Phi\,.\end{aligned} \tag{29}$$

Here, the mean frequency ω_p is the same as in (15); correlation factors f_p are expressed via the correlative Onsager coefficients L^c_{pq} in Eqs. (27) as follows:

$$\begin{aligned}f_A &= 1-\left(\frac{\omega_B}{\omega_A}c_A L^c_{AB} + cL^c_{AA}\right),\\ f_B &= 1-\left(c_A L^c_{BB} + cL^c_{AB}\right),\end{aligned} \tag{30}$$

and Φ is the "thermodynamic factor" [2]. The PCA expression for this factor is given by Eq. (42) in [30].

The chemical interdiffusion coefficient D_{chem} is expressed via D_p in (29) as follows:

$$\begin{aligned}D_{chem} &= (c_A n\bar{v}_A D_B + cn\bar{v}_B D_A) =\\ &= a_0^2(c_A\omega_B f_B + c\,\omega_A f_A)\Phi.\end{aligned} \tag{31}$$

The tracer diffusion coefficient D_{p^*} with p^* corresponding to either tracer solvent atoms A^* or tracer solute atoms B^* can be written in the form (29) with replacing p by p^* and omitting factors $n\overline{v}_p$ and Φ [30]:

$$D_{p^*} = a_0^2\omega_p f_{p^*}, \tag{32}$$

where ω_p is the same as in (29) and f^*_p is the tracer correlation factor. Explicit equations for tracer correlation factors in the kinetic mean-field approximation used below will be presented in Sec. 5.

Equations (29) and (32) show that each diffusion coefficient D_p or D_{p^*} has the form of product of the mean frequency of vacancy-atom exchange, ω_p, and the appropriate correlation factor f_p or f^*_p (saying not about standard geometrical or thermodynamic factors). Concentration dependence of these two factors will be shown below to be usually very different: dependences $\omega_p(c)$ are typically very sharp, while dependences $f_p(c)$ and $f^*_p(c)$ are much weaker. It will qualitatively explain sharp concentration dependences of diffusion coefficients typical of real alloys.

Equations (10)–(32) provide a basis for the statistical theory of diffusion in concentrated alloys. In Secs. 3–6, we describe explicit form of these equations for BCC and FCC alloys in different approximations.

3. CORRELATION OPERATORS $\hat{b}^p_{01}$ FOR BCC AND FCC ALLOYS WITH ARBITRARY PAIRWISE INTERACTION

In the previous works [29, 30], we used the nearest-neighbor-interaction (NNI) model of FCC alloys for which both kinetic interactions u^λ_{il} and saddle-point interactions $\Delta^{\lambda l}_{p,ij}$ in the correlation operator $\hat{b}^p_{01}$ (13) act only between nearest-neighbors. In this section, we discuss the form of this operator for BCC and FCC alloys with any pairwise kinetic and saddle-point interactions and illustrate resulting expressions by examples of three-neighbor interaction (3NI) models.

To this end, it is convenient to express the correlation operator $\hat{b}^p_{01}$ (13) in terms of the "correlation Hamiltonian" $H^c_{p,01}$ which describes influence of kinetic and saddle-point interactions between neighboring atoms on the $p0 \leftrightharpoons v1$ jump probability. This correlation Hamiltonian has the form of a sum of interactions with different groups of sites i_ξ having the same crystal symmetry ξ (with respect to the bond (0,1) of the $p0 \leftrightharpoons v1$ jump) described by the correlation energy $\varepsilon^\alpha_{p\xi}$:

$$\begin{aligned}\hat{b}^p_{01} &= n^h_0 n^h_1 \exp\left(\beta H^c_{p,01}\right),\\ H^c_{p,01} &= \sum_{\alpha,\xi}\varepsilon^\alpha_{p\xi}\sum_{i_\xi} n^\alpha_{i_\xi}.\end{aligned} \tag{33}$$

Positions $\mathbf{R}_i$ and symmetries ξ of all sites $i = i_\xi$ in Eqs. (33) considered below for BCC and FCC alloys are presented in Tables A3–A6 in Appendix 1. Each symmetry ξ can be conveniently characterized by the numbers m and n of coordination spheres for the lattice

vectors $\mathbf{R}_m$ and $\mathbf{R}_n$ which describe the position $\mathbf{R}_i$ of site $i = i_\xi$ with respect to two "central" sites, 0 and 1,

$$\mathbf{R}_m = \mathbf{R}_i - \mathbf{R}_0, \quad \mathbf{R}_n = \mathbf{R}_i - \mathbf{R}_1;$$

or

$$\mathbf{R}_m = \mathbf{R}_i - \mathbf{R}_1, \quad \mathbf{R}_n = \mathbf{R}_i - \mathbf{R}_0. \tag{34}$$

For sites 0 and 1 corresponding to the $p0 \leftrightharpoons v1$ jump under consideration, the symmetry ξ is denoted in Tables A3–A6 as $\xi = j$ (implying: "jumping"). For other sites $i \neq 0, 1$, symmetries ξ are described by Latin letters $l = a, b, c, \ldots$, in the order of increasing the values m and n in Eqs. (34). If sites i with different symmetries ξ correspond to the same energy $\varepsilon^\alpha_{p\xi}$ in the Hamiltonian (33), such symmetries can be denoted as l_n, with the same letter l and the same energy $\varepsilon^\alpha_{l_n} = \varepsilon^\alpha_l$ in Eq. (33) but with different numerical indices n. For the 3NI model, such symmetries in Tables A3–A6 are e_1, e_2 and $f_1, f_2, \ldots, f_6$ for BCC alloys, or $h_1, h_2, \ldots, h_4$ and i_1, i_2, i_3 for FCC alloys, while the appropriate energies in (33) are ε^α_e and ε^α_f or ε^α_h and ε^α_i. The value $N(i_\xi)$ in the last line of Table A3 or A4 is the total number of sites i_ξ for each symmetry ξ.

For a BCC alloy, sites i_ξ with $\xi = a, b, c$ are the nearest neighbors of site 0 or site 1, as shown in Fig. 1:

$$\begin{aligned} &i_a = 2, 4, 5, \bar{3}, \bar{6}, \bar{8}; \quad i_b = 3, 6, 8, \bar{2}, \bar{4}, \bar{5}; \\ &i_c = 7, \bar{1}. \end{aligned} \tag{35}$$

For an FCC alloy, symmetries ξ denoted in Table A2 as a, b, c, d (and in paper [29] as Δ, v, s, c) correspond to the nearest neighbors of site 0 or (and) site 1, as shown in Fig. 2:

$$\begin{aligned} &i_a = 2, 4, 9, 12; \quad i_b = \ 3, 5, \bar{3}, \bar{5}; \\ &i_c = 6, 8, 10, 11, \bar{2}, \bar{4}, \bar{9}, \bar{12}; \quad i_d = 7, \bar{1}. \end{aligned} \tag{36}$$

For the 3NI model of a BCC alloy, correlation energies $\varepsilon^\alpha_{p\xi}$ in (33) are expressed via kinetic interactions u^α_n and saddle-point interactions Δ^α_{np} for the n-th neighbors as follows:

$$\begin{aligned} &\varepsilon^\alpha_{pa} = u^\alpha_1 + u^\alpha_2 - \Delta^\alpha_{1p}, \quad \varepsilon^\alpha_{pb} = u^\alpha_1 + u^\alpha_3 - \Delta^\alpha_{2p}, \\ &\varepsilon^\alpha_{pc} = u^\alpha_1 - \Delta^\alpha_{3p}, \quad \varepsilon^\alpha_{pd} = u^\alpha_2 - \Delta^\alpha_{4p}, \\ &\varepsilon^\alpha_{pe} = u^\alpha_3, \quad \varepsilon^\alpha_{pf} = 0. \end{aligned} \tag{37}$$

Here, index p at energies $\varepsilon^\alpha_{p\xi}$ which do not depend on the kind p of a jumping atom (do not include the saddle-point energy Δ^α_{np}) can be omitted, but we preserve it for uniformity of notation. The saddle-point energies $\Delta^\alpha_{np} = \Delta^\alpha_p(\mathbf{R}_{ns})$ correspond to the following vectors $\mathbf{R}_{ns} = \mathbf{R}_{i_n} - \mathbf{R}_s$ which describe displacements of site i_n with respect to the saddle point $\mathbf{R}_s = (0.5, 0.5, 0.5)$ (in $a_0/2$ units, here and below):

$$\begin{aligned} &\mathbf{R}_{1s} = (0.5, 0.5, -1.5), \quad \mathbf{R}_{2s} = (1.5, 1.5, -0.5), \\ &\mathbf{R}_{3s} = (1.5, 1.5, 1.5), \quad \mathbf{R}_{4s} = (0.5, 0.5, 2.5). \end{aligned} \tag{38}$$

In Eqs. (37) and (38), we take into account that interatomic distances for the saddle-point interactions Δ^α_{3p} and Δ^α_{4p} are the same: $R_{3s} = R_{4s} = (27/4)^{1/2}$, and we allow for both these interactions. The NNI (or "four-frequency") model of BCC alloys in Eqs. (37) corresponds to $\varepsilon_b = \varepsilon_c$ and $\varepsilon_d = \varepsilon_e = 0$.

For the 3NI model of an FCC alloy, correlation energies $\varepsilon^\alpha_{p\xi}$ in (33) are

$$\begin{aligned} &\varepsilon^\alpha_{pa} = 2u^\alpha_1 - \Delta^\alpha_{1p}, \quad \varepsilon^\alpha_{pb} = u^\alpha_1 + u^\alpha_2 - \Delta^\alpha_{2p}, \\ &\varepsilon^\alpha_{pc} = u^\alpha_1 + u^\alpha_3 - \Delta^\alpha_{3p}, \quad \varepsilon^\alpha_{pd} = u^\alpha_1, \\ &\varepsilon^\alpha_{pe} = u^\alpha_2 + u^\alpha_3, \quad \varepsilon^\alpha_{pf} = u^\alpha_2, \\ &\varepsilon^\alpha_{pg} = 2u^\alpha_3, \quad \varepsilon^\alpha_{ph} = u^\alpha_3, \quad \varepsilon^\alpha_{pi} = 0, \end{aligned} \tag{39}$$

where the saddle-point energy $\Delta^\alpha_{np} = \Delta^\alpha_p(\mathbf{R}_{ns})$ corresponds to the following vector $\mathbf{R}_{ns}$ of displacement of site i_n with respect to the saddle point $\mathbf{R}_s = (0, 0.5, 0.5)$:

$$\begin{aligned} &\mathbf{R}_{1s} = (1, -0.5, -0.5), \quad \mathbf{R}_{2s} = (0, 1.5, -0.5), \\ &\mathbf{R}_{3s} = (1, 0.5, 1.5). \end{aligned} \tag{40}$$

The NNI (or "five-frequency" [2]) model of FCC alloys in Eqs. (39) corresponds to $\varepsilon_b = \varepsilon_c = \varepsilon_d$ and $\varepsilon_{e,f,g,h} = 0$.

Let us also note that due to the operator identities

$$n^\alpha_i n^p_i = n^\alpha_i \delta_{\alpha p}, \quad \exp(x n^\alpha_i) = 1 + n^\alpha_i f(x), \tag{41}$$

where $\delta_{\alpha p}$ is the Kroneker symbol and $f(x)$ is $(e^x - 1)$, each factor $\exp(\beta \varepsilon^\alpha_\xi n^\alpha_{i_\xi})$ in the correlation operator (33) can be written as

$$\exp(\beta \varepsilon^\alpha_\xi n^\alpha_{i_\xi}) = 1 + n^\alpha_{i_\xi} f^\alpha_{p\xi},$$

where

$$f^\alpha_{p\xi} = e^\alpha_{p\xi} - 1, \quad e^\alpha_{p\xi} = \exp(\beta \varepsilon^\alpha_{p\xi}). \tag{42}$$

It leads to the following two relations used in the calculations below:

$$\begin{aligned} &n^\alpha_{i_\xi} \exp\left(\beta \sum_\lambda \varepsilon^\lambda_{p\xi} n^\lambda_{i_\xi}\right) = n^\alpha_{i_\xi} e^\alpha_{p\xi}, \\ &n^h_{i_\xi} \exp\left(\beta \sum_\lambda \varepsilon^\lambda_{p\xi} n^\lambda_{i_\xi}\right) = n^h_{i_\xi}. \end{aligned} \tag{43}$$

4. DESCRIPTION OF VACANCY CORRELATIONS AND EXPRESSIONS FOR COEFFICIENTS IN BASIC EQUATIONS (17) AND (19) VIA STATISTICAL AVERAGES

As mentioned in Sec. 2, the pairwise vacancy correlation effects in the master equation approach are described by effective interactions ("fields") $h_n^{\rho\lambda}$ in Eqs. (17) and (19). Different approximations in description of these effects correspond to different choices of the total number n_{max} of such fields [24, 29], and using higher n_{max} enables one to describe these effects more accurately.

The simplest approximation, to be called the nearest-neighbor-jump approximation (NNJA), corresponds to $n_{max} = 1$ and to presence in Eqs. (17)–(20) of only one vector $\mathbf{R}_{n,1} = \mathbf{R}_{1,1}$. This approximation is usually sufficient for qualitative description of vacancy correlations with the typical accuracy of the order of 10–20 %. For quantitative descriptions, we will use the "second-shell-jump approximation" (SSJA) which takes into account vacancy correlations for all sites which can be reached by a vacancy for two jumps. The SSJA has been first suggested by Bocquet [1] for dilute FCC alloys. For BCC alloys, SSJA correspond to $n_{max} = 6$, and for FCC alloys, to $n_{max} = 5$.

For the SSJA, vectors $\mathbf{R}_{n,1}$ in Eqs. (17)–(20) can be chosen as follows:

$$\begin{aligned}&\text{BCC alloys:}\\ &\quad\{\mathbf{R}_{1,1};\mathbf{R}_{2,1};\mathbf{R}_{3,1};\mathbf{R}_{4,1};\mathbf{R}_{5,1};\mathbf{R}_{6,1}\} =\\ &\quad=\{111;002;022;131;113;222\};\\ &\text{FCC alloys:}\\ &\quad\{\mathbf{R}_{1,1};\mathbf{R}_{2,1};\mathbf{R}_{3,1};\mathbf{R}_{4,1};\mathbf{R}_{5,1}\} =\\ &\quad=\{011;002;121;112;022\}.\end{aligned} \tag{44}$$

Below in this section, we derive expressions for coefficients $l_{p,n}^{\lambda}$, $m_{p,n}^{q}$ and $t_{p,nm}^{q\lambda}$ in Eqs. (17) and (19) via one-site and two-site averages (23). Note that terms with the occupation operators n_i^q for sites $i = 0$ and $i = 1$ are actually absent in these expressions due to the condition $k \neq 0 \neq j$ in basic equations (16).

First, we consider coefficients $l_{p,n}^{\lambda}$, $m_{p,n}^{q}$, and $t_{1p,nm}^{q}$ in Eqs. (18), (20), and (24) which are expressed via one-site averages ν_{pi}^{q} in (23). Each such average evidently depends only on the symmetry ξ of site i but not on the choice of this site among all sites of this symmetry: $\nu_{pi_\xi}^{q} = \nu_{p\xi}^{q}$. Then, using Tables A1 and A2 for operators of turn $\hat{T}_k$, we can express coefficients $m_{p,n}^{q}$ in Eqs. (21) via averages $\nu_{p\xi}^{q}$ as follows:

$$\begin{aligned}&\text{BCC:}\\ &\quad m_{p,1}^{q} = (\nu_a - \nu_b - \nu_c)_p^q, \quad m_{p,2}^{q} = 4(\nu_a - \nu_d)_p^q,\\ &\quad m_{p,3}^{q} = 2(\nu_b - \nu_{e_2})_p^q,\\ &\quad m_{p,4}^{q} = (\nu_d + \nu_{f_2} - \nu_{f_1} - \nu_{f_4})_p^q,\\ &\quad m_{p,5}^{q} = (\nu_d + 2\nu_{e_1} + \nu_{f_1} - \nu_{f_2} - 2\nu_{f_3} - \nu_{f_4})_p^q,\\ &\quad m_{p,6}^{q} = (\nu_c + \nu_{f_1} - \nu_{f_5} - \nu_{f_6})_p^q;\\ &\text{FCC:}\\ &\quad m_{p,1}^{q} = (2\nu_a - 2\nu_c - \nu_d)_p^q, \quad m_{p,2}^{q} = 4(\nu_b - \nu_f)_p^q,\\ &\quad m_{p,3}^{q} = (\nu_c + \nu_e + \nu_{h_2} - \nu_g - \nu_{h_3} - \nu_{h_4})_p^q,\\ &\quad m_{p,4}^{q} = 2(\nu_c + \nu_g - \nu_{h_2} - \nu_{h_4})_p^q,\\ &\quad m_{p,5}^{q} = (\nu_d + 2\nu_{h_1} - 2\nu_{i_2} - \nu_{i_3})_p^q.\end{aligned} \tag{45}$$

Here, symmetries $\xi = a, b, \ldots$ are indicated in Tables A3–A6 and indices q and p at brackets mean that they should be put at each term within brackets, e. g. $(\nu_a + \ldots)_p^q = (\nu_{pa}^q + \ldots)$. In a binary alloy AB, due to the identity $(n_i^A + n_i^B) = 1$, coefficients $m_{p,n}^{q}$ (21) obey following relations being useful for calculations:

$$m_{p,n}^{A} + m_{p,n}^{B} = -c\omega_p\delta_{n1}, \tag{46}$$

where δ_{n1} is Kroneker symbol.

Calculations of coefficients $l_{p,n}^{q}$ in Eqs. (18) using Tables A3–A6 show that each $l_{p,n}^{q}$ differs from the analogous coefficient $m_{p,n}^{q}$ in (45) just by a constant C_n:

$$l_{p,n}^{q} = 2C_n m_{p,n}^{q}, \tag{47}$$

where constants C_n for different n are as follows

$$\begin{aligned}&\text{BCC alloy:}\\ &\quad C_{1,3,5,6} = 1; \quad C_2 = 1/4; \quad C_4 = 2;\\ &\text{FCC alloy:}\\ &\quad C_{1,4,5} = 1; \quad C_2 = 1/4; \quad C_3 = 2.\end{aligned} \tag{48}$$

Expressions for terms $t_{1p,nm}^{q}$ in Eq. (24) via one-site averages can be found using Eq. (22) and conditions of coincidence of operator $n_{n,1}^{q}$ with some of operators n_i^{λ} in the sum $\sigma_{k,m}^{\lambda}$ in (22). These expressions are presented in Appendix 2.

To write the two-site terms $t_{2p,nm}^{q\lambda}$ in Eq. (24), we note that due to the crystal symmetry, terms $\hat{T}_k\sigma_{k,m}^{\lambda}$ in Eq. (22) for a number of different values k are equal to each other or differ only by the sign. It enables us to write Eq. (22) as follows:

$$t_{p,nm}^{q\lambda} = \langle \hat{w}_{01}^{p}(\varphi_{Am}^{\lambda}\hat{T}_A + \varphi_{Bm}^{\lambda}\hat{T}_B + \varphi_{Cm}^{\lambda}\hat{T}_C)\, n_{n,1}^{q}\rangle. \tag{49}$$

Here, operators $\hat{T}_L$ and φ^{λ}_{Lm} with L equal to A, B, or C are expressed via operators of turn $\hat{T}_k$ and terms $\sigma^{\lambda}_{k,m}$ in Eq. (22) as follows:

$$\begin{aligned}
&\text{BCC:}\\
&\hat{T}_A = \hat{T}_1 + \hat{T}_2 + \hat{T}_3 + \hat{T}_4, \quad \hat{T}_B = \hat{T}_5,\\
&\hat{T}_C = \hat{T}_6 + \hat{T}_7 + \hat{T}_8;\\
&\varphi^{\lambda}_{Am} = \sigma^{\lambda}_{1,m}, \quad \varphi^{\lambda}_{Bm} = \hat{T}_5\sigma^{\lambda}_{5,m},\\
&\varphi^{\lambda}_{Cm} = \hat{T}_6\sigma^{\lambda}_{6,m};\\
&\text{FCC:}\\
&\hat{T}_A = \hat{T}_1 + \hat{T}_2 + \hat{T}_3 + \hat{T}_4 - \hat{T}_7,\\
&\hat{T}_B = \hat{T}_5 + \hat{T}_6 + \hat{T}_8,\\
&\hat{T}_C = \hat{T}_9 + \hat{T}_{10} - \hat{T}_{11} - \hat{T}_{12};\\
&\varphi^{\lambda}_{Am} = \sigma^{\lambda}_{1,m}, \quad \varphi^{\lambda}_{Bm} = \hat{T}_5\sigma^{\lambda}_{5,m},\\
&\varphi^{\lambda}_{Cm} = \hat{T}_9\sigma^{\lambda}_{9,m}.
\end{aligned} \tag{50}$$

The form of expressions for two-site terms $t^{q\lambda}_{2p,nm}$ in (24) via averages $\nu^{q\lambda}_{p,ij}$ in (23) can be illustrated by the term $t^{q\lambda}_{2p,11}$ used in the NNJA. It can be written as the sum of terms $t_{\xi\xi'}$ corresponding to different symmetries ξ and $\xi^{'}$ of sites i and j:

$$t^{q\lambda}_{2p,11} = \sum_{\xi,\xi'} t_{\xi\xi'}. \tag{51}$$

In the notation of Sec. 3, symmetries ξ and $\xi^{'}$ in (51) correspond to a, b, or c for BCC alloys, and a, b, c, or d for FCC alloys, while $t_{\xi\xi'}$ can be written as follows:

$$\begin{aligned}
&\text{BCC alloys:}\\
&t_{aa} = 3\nu_{2\bar{8}} - 2\nu_{2\bar{5}} - 2\nu_{2\bar{3}},\\
&t_{ab} = 2\nu_{23} - 3\nu_{2\bar{8}} - 3\nu_{2\bar{2}} + 2\nu_{2\bar{5}},\\
&t_{ac} = -(\nu_{27} + \nu_{2\bar{1}}),\\
&t_{bb} = 3\nu_{3\bar{5}} - 2\nu_{36} - 2\nu_{3\bar{4}},\\
&t_{bc} = \nu_{37} + \nu_{3\bar{1}}, \quad t_{cc} = \nu_{7\bar{1}};\\
&\text{FCC alloys:}\\
&t_{aa} = 2(\nu_{24} + \nu_{29} + \nu_{49}),\\
&t_{ac} = -2(\nu_{26} + \nu_{28} + \nu_{2,10} + \nu_{2,11}),\\
&t_{ad} = -4\nu_{27},\\
&t_{bb} = 2(\nu_{3\bar{5}} - \nu_{35} - \nu_{3\bar{3}}),\\
&t_{bc} = 2(\nu_{3,10} - \nu_{36} - \nu_{3\bar{2}} + \nu_{3\bar{9}}),\\
&t_{cc} = 2(\nu_{6,10} + 2\nu_{6\bar{4}} - \nu_{6,11} - \nu_{6\bar{9}} - \nu_{6,\bar{1}2}),\\
&t_{cd} = 2(\nu_{67} + \nu_{6\bar{1}}), \quad t_{dd} = \nu_{7\bar{1}}\,.
\end{aligned} \tag{52}$$

Here, ν_{ij} or $\nu_{i,j}$ means $\nu^{q\lambda}_{p,ij}$ and terms $t_{\xi'\xi}$ with $\xi^{'} \neq \xi$ not given in (52) are obtained from terms $t_{\xi\xi'}$ presented in these equations by interchanging indices q and λ. Expressions for terms $t^{q\lambda}_{2p,nm}$ with all n and m used in SSJA are given in Appendix 3 for the kinetic mean-field approximation described below.

5. CALCULATIONS OF STATISTICAL AVERAGES USING KINETIC MEAN-FIELD APPROXIMATION

Statistical averages in Eqs. (15) and (23) can be evaluated using either Monte Carlo simulations discussed in Sec. 6 or approximate analytical calculations. In this section, we describe the simple and effective method of such calculations, the kinetic mean-field approximation (KMFA) suggested in Refs. [29, 30]. For dilute alloys, KMFA is exact, while comparison with Monte Carlo simulations made in [30] and in Sec. 6 shows that it is usually sufficiently accurate for all concentrations. Below, we present main relations of KMFA for the case of arbitrary pairwise interactions considered in this work.

The KMFA neglects fluctuations of occupation numbers n^p_i in statistical averages (15) and (23): each n^p_i is replaced by its mean value $\langle n^p_i\rangle = c_p$. At the same time, thermodynamic quantities, in particular, thermodynamic activity coefficients a_α in Eqs. (11), are found using the more exact, pair-cluster approximation (PCA). For example, for a binary alloy AB, the PCA expression for a_B (related to the thermodynamic factor Φ in Eq. (29) as $\Phi = 1 + cc_A d\ln a_B/dc$) has the form

$$a_B = \frac{c_A}{c}\exp(\beta\lambda_B) = \\ = \exp\left\{-\sum_{n=1} z_n \ln\left(1 + \frac{2cf^{BB}_n}{R_n + 1}\right)\right\}, \tag{53}$$

where f^{BB}_n is $[\exp(-\beta v^{BB}_n) - 1]$, R_n is $(1 + 4cc_A f^{BB}_n)^{1/2}$, z_n is the coordination number for the n-th shell in the crystal, and v^{BB}_n is the "thermodynamic" solute-solute interaction in this shell.

5.1. KMFA expressions for mean frequencies

Let us first find KMFA expressions for mean frequencies ω_p in (15). To this end, we can use Eqs. (10)–(12), (33), and (41). Using also Eqs. (10) and (33) for the operator $\hat{w}^p_{01}$ in the average (15) and replacing each n^p_i in this average by its mean value $\langle n^p_i\rangle = c_p$, we obtain the KMFA expressions for mean frequencies ω_p (to be denoted ω^0_p) which generalizes Eqs. (24) in [30] for NNI model to the case of arbitrary pairwise interactions:

$$\omega_\alpha^0 = \omega_{\alpha 0} a_\alpha \prod_\xi S_{\alpha\xi}^{N_\xi}, \quad \omega_h^0 = \omega_{h0} \prod_\xi S_{h\xi}^{N_\xi}, \tag{54}$$

where ω_{p0} is the same as in (12). Each factor $S_{p\xi}$ in (54) is expressed via Mayer functions $f_{p\xi}^\alpha$ for correlation energies $\varepsilon_{p\xi}^\alpha$ in Eq. (33) as follows:

$$S_{p\xi} = 1 + \sum_\alpha c_\alpha f_{p\xi}^\alpha, \tag{55}$$

where $f_{p\xi}^\alpha$ and $e_{p\xi}^\alpha$ are the same as in (42). Value N_ξ in Eq. (54) is the total number of sites i with the energy $\varepsilon_{p\xi}^\alpha$ in the correlation Hamiltonian (33). For symmetries ξ for which energies $\varepsilon_{p\xi}^\alpha$ differ from each other, this N_ξ coincides with $N(i_\xi)$ in Tables 1 and 2. If symmetries $\xi = l_n$ correspond to the same correlation energy $\varepsilon_{p\xi}^\alpha$ for several l_n (as it is for symmetries e_n and f_n or h_n and i_n for the 3NI model used in Sec. 3), value N_ξ in (54) is the sum of $N(i_{l_n})$ over all l_n.

For the 3NI model, Eqs. (54) at any p can be explicitly written as follows:

$$\begin{aligned} &\text{BCC:}\\ &\quad \omega_p^0 = \omega_{p0} a_p S_{pa}^6 S_{pb}^6 S_{pc}^2 S_{pd}^6 S_{pe}^{18},\\ &\text{FCC:}\\ &\quad \omega_p^0 = \omega_{p0} a_p S_{pa}^4 S_{pb}^4 S_{pc}^8 S_{pd}^2 S_{pe}^4 S_{pf}^4 S_{pg}^8 S_{ph}^{20}, \end{aligned} \tag{56}$$

where we put for brevity $a_h = 1$. Expressions (56) generalize Eqs. (68) of Ref. [29] derived for the NNI model of FCC alloys (for which we have in the second equation in (56): $S_{pb} = S_{pc} = S_{pd}$, $S_{pe,pg,pf,ph} = 1$).

Expressions (54)–(56) show that at not weak correlation energies $\varepsilon_{p\xi}^\alpha$ in (42) typical of real alloys, concentration dependences of mean frequencies ω_p^0, generally, should be very sharp, due to the presence in these expressions of many factors $S_{p\xi}^{N_\xi}$ with high exponents N_ξ. These high exponents have mainly a geometrical origin related to a high number of neighbors of each bond in the close-packed BCC and FCC structures. When correlation energies $\varepsilon_{p\xi}^\alpha$ are mainly positive (in particular, when kinetic interactions u_n^α in Eqs. (37) and (37) are mainly positive), mean frequencies increase with concentrations c_α; for negative $\varepsilon_{p\xi}^\alpha$ and u_n^α, types of these concentration dependences change sign. It is illustrated by the results for alloys CuNi, CuZn, and AgCd presented in Ref. [30].

Expressions for correlation factors $f_p(c)$ and $f_{p^*}(c)$ discussed below do not include such sharp factors as Eqs. (54) and (56), they depend on one-site and two-site averages given by (23) and (57), and these factors usually vary with concentration c rather smoothly, as illustrated by Fig. 4 below.

As discussed in Ref. [30] and in Sec. 6, KMFA results (54) and (56) for mean frequencies are usually sufficiently close to exact values $\omega_p(c)$. Hence sharp concentration dependences of diffusion coefficients typical of real alloys are mainly explained by these KMFA results for mean frequencies $\omega_p(c)$ in Eqs. (29), (32) and analogous relations.

5.2. KMFA expressions for one-site and two-site averages

To describe effects of vacancy correlations on diffusion, we should find one-site and two-site averages ν_{pi}^q and $\nu_{p,ij}^{q\lambda}$ in (23) which enter quantities $m_{p,n}^q$, $l_{p,n}^q$, $t_{1p,nm}^q$, $t_{2p,nm}^{q\lambda}$ in Eqs. (45)–(49). KMFA expressions for these averages will be denoted by the upper index "0", just as for ω_p^0 in (54), and these expressions can be conveniently written in terms of "reduced" quantities marked by the upper symbol "tilde":

$$\begin{aligned} &\{\nu_{pi}^q,\, m_{p,n}^q,\, l_{p,n}^q,\, t_{1p,nm}^q\}^0 =\\ &= c_p c_q \omega_p^0 \cdot \{\tilde\nu_{pi}^q,\, \tilde m_{p,n}^q,\, \tilde l_{p,n}^q,\, \tilde t_{1p,nm}^q\},\\ &\{\nu_{p,ij}^{q\lambda},\, t_{2p,nm}^{q\lambda}\}^0 = c_p c_q c_\lambda \omega_p^0 \cdot \{\tilde\nu_{p,ij}^{q\lambda},\, \tilde t_{2p,nm}^{q\lambda}\}. \end{aligned} \tag{57}$$

To find "reduced" averages $\tilde\nu_{pi}^q$ and $\tilde\nu_{p,ij}^{q\lambda}$ in (57), we can use relations (10), (23), (33), and (43). Employing the same arguments as in derivation of KMFA expressions (54) for frequencies, we obtain

$$\tilde\nu_{pi}^q = \eta_{p\xi}^q; \quad \tilde\nu_{p,ij}^{q\lambda} = \eta_{p\xi}^q \eta_{p\xi'}^\lambda. \tag{58}$$

Here, index ξ or ξ' indicates symmetry of site i or site j, while the factor $\eta_{p\xi}^q$ is expressed via quantities $e_{p\xi}^\alpha$ and $S_{p\xi}$ in Eqs. (42) and (55) as follows:

$$\eta_{p\xi}^\alpha = \frac{e_{p\xi}^\alpha}{S_{p\xi}}, \quad \eta_{p\xi}^h = \frac{1}{S_{p\xi}}. \tag{59}$$

KMFA expressions for reduced quantities $\tilde m_{p,n}^q$, $\tilde l_{p,n}^q$, $\tilde t_{1p,nm}^q$, and $\tilde t_{2p,nm}^{q\lambda}$ in Eqs. (57) can be obtained using relations (45)–(49), (58), and (97)–(105) in Appendix 2. In particular, to find one-site quantities $\tilde m_{p,n}^q$, $\tilde l_{p,n}^q$, or $\tilde t_{1p,nm}^q$, we should just replace each $\nu_{p\xi}^q$ in Eqs. (45), (47), or (97)–(100) by $\eta_{p\xi}^q$ from Eq. (59). For example, KMFA expressions for quantities $\tilde m_{p,1}^q$ and $\tilde t_{1p,11}^q$ used in the NNJA are as follows:

$$\begin{aligned} &\text{BCC alloys:}\\ &\quad \tilde m_{p,1}^q = (\eta_a - \eta_b - \eta_c)_p^q,\\ &\quad \tilde t_{1p,11}^q = (3\eta_a + 3\eta_b + \eta_c)_p^q;\\ &\text{FCC alloys:}\\ &\quad \tilde m_{p,1}^q = (2\eta_a - 2\eta_b - \eta_d)_p^q,\\ &\quad \tilde t_{1p,11}^q = (2\eta_a + 2\eta_b + 4\eta_c + \eta_d)_p^q. \end{aligned} \tag{60}$$

KMFA expressions for two-site quantities $\tilde t_{2p,nm}^{q\lambda}$ are given by Eqs. (102)–(105) in Appendix 3.

5.3. KMFA expressions for mean frequencies and correlation factors in binary alloys

In Secs. 5.1 and 5.2, we considered alloys with any number of components. For a binary alloy AB, index α in Eqs. (55) and (59) takes the only value $\alpha = B$, to be omitted for brevity:

$$f^B_{p\xi} = f_{p\xi} = e_{p\xi} - 1, \quad S_{p\xi} = 1 + cf_{p\xi},$$
$$\eta^B_{p\xi} = \eta_{p\xi} = \frac{e_{p\xi}}{S_{p\xi}}, \quad \eta^A_{p\xi} = \frac{1}{S_{p\xi}}. \tag{61}$$

To make more clear relations between factors $e_{p\xi}$ in (61) and kinetic or saddle-point interactions u^B_n or Δ^B_{np} in Eqs. (37) and (39), we also present expressions for $e_{p\xi}$ via the "interaction factors" $e_n = \exp(\beta u^B_n)$ and $\zeta_{np} = \exp(-\beta\Delta^B_{np})$ for the 3NI model:

BCC alloys:
$$e_{pa} = e_1e_2\zeta_{1p}, \quad e_{pb} = e_1e_3\zeta_{2p},$$
$$e_{pc} = e_1\zeta_{3p}, \quad e_{pd} = e_2\zeta_{4p}, \quad e_e = e_3,$$
FCC alloys: (62)
$$e_{pa} = e_1^2\zeta_{1p}, \quad e_{pb} = e_1e_2\zeta_{2p},$$
$$e_{pc} = e_1e_3\zeta_{3p}, \quad e_{pd} = e_1, \quad e_e = e_2e_3,$$
$$e_f = e_2, \quad e_g = e_3^2, \quad e_h = e_3.$$

Equations (56), (61), and (62) illustrate sharp concentration dependences of mean frequencies $\omega^0_p(c)$ mentioned above.

Below in this section, we present explicit KMFA expressions for correlation factors in binary alloys. The vacancy correlation effects will be described using SSJA or NNJA which seem usually to be sufficiently accuirate.

First we consider tracer diffusion and present the KMFA equations for correlation factors f_{p^*} derived in Ref. [30] (which can be shown to be true not only for the NNI model used in Ref. [30] but for arbitrary pairwise interactions). The tracer solvent correlation factor f_{A^*} is expressed via appropriate effective fields $h^{A^*v}_n$ and $h^{A^*B}_n$ as follows:

$$f_{A^*} = 1 - 2c_A\tilde{m}^A_{A,1}\tilde{h}^{A^*v}_1 - 2c\,\tilde{m}^B_{A,1}(\tilde{h}^{A^*v}_1 - \tilde{h}^{A^*B}_1) + c\sum_{n=2}^{n_{max}}\tilde{l}^B_{A,n}\tilde{h}^{A^*B}_n. \tag{63}$$

Here, quantities $\tilde{m}^q_{p,n}$, $\tilde{t}^q_{1p,nm}$, and $\tilde{t}^{qq'}_{2p,nm}$ are the same as in Eqs. (57), while fields $h^{A^*v}_n$ and $h^{A^*B}_n$ are determined by the following set of equations:

$$\sum_{m=1}^{n_{max}}[\tilde{h}^{A^*v}_m(\tilde{t}^A_{1A,nm} - 2\delta_{m1}\tilde{m}^A_{A,n}) - c\tilde{h}^{A^*B}_m\tilde{t}^{AB}_{2A,nm}] = \tilde{m}^A_{A,n},$$
$$\sum_{m=1}^{n_{max}}[\tilde{h}^{A^*v}_m(z\tilde{t}^A_{1B,nm} - 2\delta_{m1}\tilde{m}^B_{A,n}) - \tilde{h}^{A^*B}_m(\tilde{t}^B_{1A,nm} + c\tilde{t}^{BB}_{2A,nm} + z\tilde{t}^A_{1B,nm})] = \tilde{m}^B_{A,n}. \tag{64}$$

Similarly, the tracer solute correlation factor f_{B^*} is expressed via appropriate effective fields $h^{B^*v}_n$ and $h^{B^*B}_n$ as follows:

$$f_{B^*} = 1 - 2c_A\tilde{m}^A_{B,1}\tilde{h}^{B^*v}_1 + 2c\tilde{m}^B_{B,1}(\tilde{h}^{B^*B}_1 - \tilde{h}^{B^*v}_1) + c\sum_{n=2}^{n_{max}}\tilde{l}^B_{B,n}\tilde{h}^{B^*B}_n, \tag{65}$$

where fields $\tilde{h}^{B^*v}_n$ and $\tilde{h}^{B^*B}_n$ obey equations analogous to (64):

$$\sum_{m=1}^{n_{max}}[\tilde{h}^{B^*v}_m(\tilde{t}^B_{1A,nm} - 2\delta_{m1}z\tilde{m}^A_{B,n}) - c\tilde{h}^{B^*B}_m z\tilde{t}^{AB}_{2B,nm}] = z\tilde{m}^A_{B,n},$$
$$\sum_{m=1}^{n_{max}}[\tilde{h}^{B^*v}_m(\tilde{t}^A_{1B,nm} - 2\delta_{m1}\tilde{m}^B_{B,n}) - \tilde{h}^{B^*B}_m(2\tilde{t}^B_{1B,nm} + c\tilde{t}^{BB}_{2B,nm})] = \tilde{m}^B_{B,n}. \tag{66}$$

In Eqs. (63)–(66), quantities n_{max} and $\tilde{m}^q_{p,n}$ are the same as in Eqs. (19) and (57), while quantities $\tilde{l}^{q'}_{p,n}$ and $\tilde{t}^{qq'}_{p,nm}$ with index q' equal to A or B are obtained from $\tilde{l}^{\lambda}_{p,n}$ and $\tilde{t}^{q\lambda}_{p,nm}$ in Eqs. (18) and (20) by replacing index λ by this q'.

Let us now discuss the intrinsic diffusion. For a binary alloy AB, Eqs. (17)–(19) with $h = A$ and $\alpha = B$ include only fields $h^{\alpha v}_n = h^{Bv}_n$ (fields h^{BB}_n are zero due to the antisymmetry of fields $h^{\rho\sigma}_n$ in indices ρ and σ [24]), and Eqs. (19) take the form

$$\sum_{m=1}^{n_{max}}A_{nm}h^{Bv}_m = m^A_{B,n}\delta\mu_B - m^B_{A,n}\delta\mu_A,$$
$$A_{nm} = t^{BB}_{A,nm} - t^{AB}_{B,nm} - \delta_{m1}2m^A_{B,n}, \tag{67}$$

where δ_{m1} is Kroneker symbol. Below, we use reduced quantities $\tilde{A}_{nm}$ defined analogously to those in Eqs. (57):

$$A_{nm} = cc_A\omega^0_A\tilde{A}_{nm}, \quad \tilde{A}_{nm} = \tilde{A}_{1,nm} + c\tilde{A}_{2,nm},$$
$$\tilde{A}_{1,nm} = \tilde{t}^B_{1A,nm} - 2z\tilde{m}^A_{B,n}\delta_{m1}, \tag{68}$$
$$\tilde{A}_{2,nm} = \tilde{t}^{BB}_{2A,nm} - z\tilde{t}^{AB}_{2B,nm}.$$

Here, $z = \omega_B^0/\omega_A^0$ with ω_p^0 from Eqs. (54)–(56) is the frequency ratio in the KMFA:

$$z = \frac{\omega_B^0}{\omega_A^0} = z_0 a_B \prod_\xi \left(\frac{S_{B\xi}}{S_{A\xi}}\right)^{N_\xi}, \qquad (69)$$

where z_0 is ω_{B0}/ω_{A0}. Equations (61) and (62) show, in particular, that each ratio $S_{B\xi}/S_{A\xi}$ in Eq. (69) differs from unity only due to the difference between saddle-point interactions Δ_{nB}^B and Δ_{nA}^B in relations of types (37) and (39).

Let us present SSJA expressions for correlative Onsager coefficients L_{pq}^c in Eqs. (27) which determine correlation factors f_p by relations (30). To this end, it is convenient to use the shortened notation:

$$\chi_{nA} = \tilde{m}_{A,n}^B, \quad \chi_{nB} = \tilde{m}_{B,n}^A, \qquad (70)$$

where quantities $\tilde{m}_{p,n}^q$ used in the KMFA are determined by Eqs. (45), (57), and (58). Then, using Eqs. (17), (26), (45)–(47), (57)–(59), (67), and (68), we find that the correlative Onsager coefficients L_{pq}^c in (27) can be concisely written as follows:

$$\begin{aligned} &L_{AA}^c = K_{AA}, \quad L_{AB}^c = K_{AB}, \quad L_{BA}^c = K_{BA}, \\ &L_{BB}^c = zK_{BB}, \end{aligned} \qquad (71)$$

where z is the same as in (69) and K_{pq} is a bilinear form in quantities χ_{np} (70):

$$K_{pq} = \sum_{n,m=1}^{n_{max}} \chi_{np} K_{nm} \chi_{mq}. \qquad (72)$$

Here, matrix elements K_{nm} are expressed via the determinant D of matrix $\tilde{A}_{nm}$ in Eqs. (68), minors M_{nm} of this determinant, and constants C_n in (47) as follows:

$$K_{nm} = \frac{2}{D}(-)^{n+m} C_n M_{mn}, \quad D = \det||\tilde{A}_{nm}||. \qquad (73)$$

For the NNJA with $n_{max} = 1$, relations (71)–(73) take the following form:

$$\begin{aligned} L_{AA}^c &= \frac{2}{D}(\tilde{m}_{A,1}^B)^2, \\ L_{AB}^c &= L_{BA}^c = \frac{2}{D}\tilde{m}_{A,1}^B \tilde{m}_{B,1}^A, \\ L_{BB}^c &= \frac{2z}{D}(\tilde{m}_{B,1}^A)^2, \end{aligned} \qquad (74)$$

where denominator $D = D(n_{max} = 1)$ is $\tilde{A}_{11}$ in (68).

Using Eqs. (68) and (97)–(105) for matrices $\tilde{A}_{nm}$, $\tilde{t}_{1p,nm}^q$, and $\tilde{t}_{2p,nm}^{q\lambda}$, we have numerically checked that the SSJA expressions (71)–(73) for correlative Onsager coefficients in both BCC and FCC alloys obey the necessary symmetry relation $L_{AB}^c = L_{BA}^c$ [2]. Presence of this symmetry relation for any concentration and interaction model confirms consistency of the master equation approach used.

6. MONTE CARLO CALCULATIONS OF STATISTICAL AVERAGES

Employing the well-elaborated Monte Carlo methods based on Metropolis algorithm [33] enables us to find statistical averages practically exactly. In this section, we use these methods, first, to assess accuracy of KMFA calculations of mean frequencies ω_p in (15) and correlation factors f_p (30) for some realistic models of alloys and, second, to show that the PCA expressions of type (53) seem to describe thermodynamics of disordered alloys under consideration with a high accuracy.

For our Metropolis Monte Carlo simulations, we used supercells with periodic boundary conditions constructed by $40\times40\times40$ repetitions in three directions of cubic cells containing two and four lattice sites for BCC and FCC lattices respectively. Thus, total amount of lattice sites was 128000 for BCC lattice and 256000 for FCC lattice. We also performed control calculations with $80\times80\times80$ supercells and different seeds for generating pseudorandom number sequencies for some of statistical averages.

At a single Monte Carlo step positions of a randomly chosen pair of nearest neighbor atoms in crystal lattice were exchanged; 10^7 of such single Monte Carlo steps were made to achieve thermal equilibrium, after which $5\cdot10^7$ more steps were made to evaluate statistical averages.

With this set of Monte Carlo parameters, we estimate relative statistical fluctuations of our Monte Carlo results as not exceeding 0.001.

Dependencies of reduced mean frequencies $\omega_{pr} = \omega_p(c)/\omega_{A0}$ on concentration for BCC alloy FeCr are displayed in Fig. 3.

As it was the case for FCC alloys CuNi, AgCd, and CuZn considered in [30], these concentration dependences are very sharp decreasing almost 4 orders of magnitude as concentraion increases from 0 to 1. Thus, it is demonstrated again that the main contribution to the sharp dependence of diffusion coeficients on concentration is due to the corresponding sharp dependences of the mean frequencies.

Discussing mean frequencies concentration dependences for FeCr it is most natural to compare them with the corresponding quantities for FCC alloy CuNi, since these two alloys exist in a wide range of concentrations reaching values $c = 1$. We note that for BCC alloy FeCr the quality of analytical statistical approximation KMFA for calculations of mean frequencies is similar to the KMFA quality for FCC alloy CuNi considered in [30]. The largest deviations between analytical and MC results for CuNi was observed at concen-

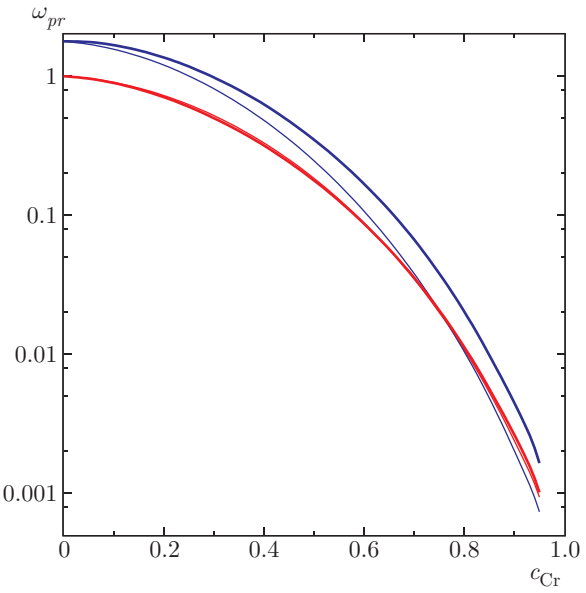

Fig. 3. (Color online) Reduced mean frequencies $\omega_{pr} = \omega_p(c)/\omega_{A0}$ in Eqs. (91) for the model of FeCr alloys described in Sec. 9. The set A in Table 2 at $T = 1573$ K is used. Thin curves correspond to KMFA and thick curves to Monte Carlo methods. Blue curves show $\omega_B^r = \omega_{\mathrm{Cr}}^r$, and red curves, $\omega_A^r = \omega_{\mathrm{Fe}}^r$

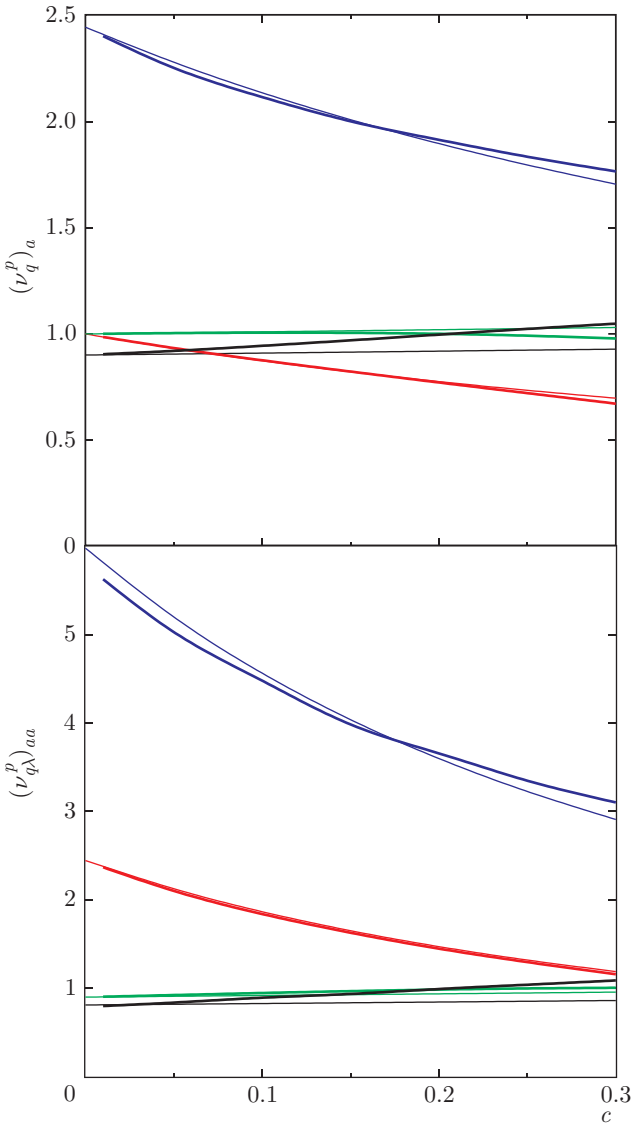

Fig. 4. (Color online) Reduced statistical averages given by formulae (23), (57), one site (upper frame) and two site (lower frame) calculated for CuZn alloy with parameters, described in [30] found using KMFA (thin curves) or NNJA and Monte Carlo (thick curves). Red lines show $\left(\tilde{\nu}_A^A\right)_a$ and $\left(\tilde{\nu}_{AB}^A\right)_{aa}$, green lines — $\left(\tilde{\nu}_B^A\right)_a$ and $\left(\tilde{\nu}_{AB}^B\right)_{aa}$, blue lines — $\left(\tilde{\nu}_A^B\right)_a$ and $\left(\tilde{\nu}_{BB}^A\right)_{aa}$, and black lines — $\left(\tilde{\nu}_B^B\right)_a$ and $\left(\tilde{\nu}_{BB}^B\right)_{aa}$

trations around $c = 0.7$–0.75, where KMFA and MC results differed by a factor of 1.6. Host atoms mean frequency for FeCr is modelled by KMFA practically exactly. For solute atoms in FeCr, alloy MC/KMFA ratio for mean frequencies is a monotonously increasing function reaching values about 2 at concentrations close to 1. At concentrations where MC/KMFA ratio reaches its largest value for CuNi, the analoguous ratio for FeCr has very close values of 1.7.

Let us now discuss accuracy of KMFA for calcuations of correlations factors. While evaluating jump frequencies requires knowledge of just correlation operator (13), correlation factors are more compelex quantities containing also one-site and two-site averages (23) and (57). NNJA and SSJA approximations used in this paper include linear combinations of these quantities with different symmetries of lattice sites given by (35) and Tables A3 and A5. Thus, to estimate KMFA accuracy for both NNJA and SSJA, we present in this section KMFA and MC concentration dependences of underlying one-site and two-site averages. Calculations were made for the model of CuZn alloy described in [30] for crystal symmetry $\xi\xi = aa$.

The maximum difference between KMFA and MC mean frequencies for CuZn alloy reported in [30] was about 10 %. The KMFA accuracy of quantities (23) and (57) shown in Fig. 4 is similar to this value or better. The only exception is $\left(\tilde{\nu}_B^{BB}\right)_{aa}$ where difference between KMFA and MC results reaches 20 %. Thus, we have demonstrated that KMFA provides good accuracy for both mean frequencies and correlations factors.

Let us now discuss accuracy of the pair-cluster approximation for description of thermodynamics of disordered BCC and FCC alloys under consideration. To this end, we will compare the PCA relation (53) for

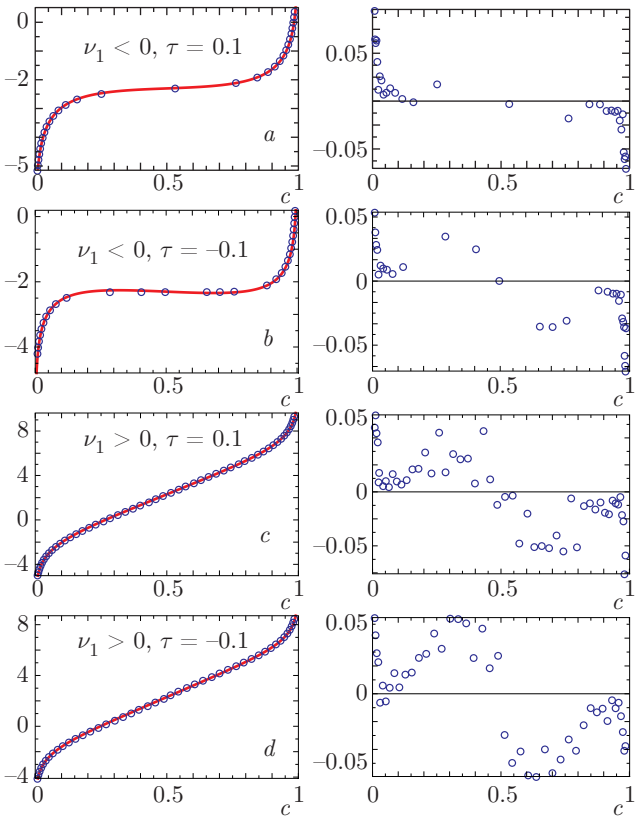

Fig. 5. (Color online) Left frames: chemical potential $\lambda_r^{\rm PCA}(c)$ in Eq. (75) (curves) and $\lambda_{\rm MC}(c)$ (blue circles), for a BCC alloy with nearest neighbor interaction found as described in text. The following values of reduced temperature τ and interaction v_1 are used. Frame a: $\tau = 0.1$, $v_1 < 0$; frame b: $\tau = -0.1$, $v_1 < 0$; frame c: $\tau = 0.1$, $v_1 > 0$; and frame d: $\tau = -0.1$, $v_1 > 0$. Each right frame shows the difference $\delta\lambda_r = \lambda_r^{\rm PCA} - \lambda_r^{\rm MC}$ (blue circles) for the same τ and v_1 values as those in the adjacent left frame

chemical potential $\lambda = \lambda^{\rm PCA}$ with the Monte Carlo results $\lambda = \lambda^{\rm MC}$. To be definite, we consider the simplest models of alloys with the nearest-neighbor thermodynamic interaction v_1. Negative v_1 correspond to the tendency to decomposition, while positive v_1 correspond to the tendency to ordering.

Comparison of functions $\lambda^{\rm PCA}(c)$ with $\lambda^{\rm MC}(c)$ for BCC alloys at some temperatures T of the order of critical temperature T_c is presented in Fig. 5. In this figure, we use reduced values of chemical potentials and temperature, λ_r and τ, in units of critical temperature found in the PCA, $T_c^{\rm PCA}$, which somewhat exceeds the exact value T_c for BCC alloys with the nearest-neighbor interaction:

$$\lambda_r = \frac{\lambda}{T_c^{\rm PCA}}, \quad \tau = \frac{T}{T_c^{\rm PCA}} - 1, \qquad T_c^{\rm PCA} = 1.59|v_1| = 1.09 T_c. \tag{75}$$

Hence values $\tau = 0.1$ or $\tau = -0.1$ considered in Fig. 5 correspond to temperatures by about 20 % above or by about 1.5 % below T_c, respectively.

Figure 5 shows that differences $\delta\lambda_r = \lambda_r^{\rm PCA} - \lambda_r^{\rm MC}$ do not exceed several percents even for $\tau = -0.1$, that is, at $T < T_c$ when the homogeneous disordered state (used in the PCA calculations) is actually thermodynamically unstable for significant intervals of concentration. This figure also shows that within the stability region, $T > T_c$, differences $\delta\lambda$ rapidly decrease when the c, T point moves off the phase boundaries, and these differences typically do not exceed about a percent. These conclusions are also true for disordered FCC alloys. Hence, the PCA seems to provide a highly accurate description of thermodynamics of BCC and FCC alloys at all concentrations and temperatures except for the narrow vicinities of phase boundaries of the disordered state.

7. SSJA AND NNJA CORRELATION FACTORS FOR DILUTE AND FOR RANDOM ALLOYS

For dilute alloys, as well as for random alloys (those with no interatomic interactions), many exact results are available. Hence, comparison of SSJA results for such alloys with these exact results can get an idea about accuracy of SSJA also for real concentrated alloys. For dilute FCC alloys, SSJA expressions for correlation factors are known only for five-frequency model [1], that is, for the nearest-neighbor interactions. For dilute BCC alloys, rather sophisticated methods to treat vacancy correlations have been developed [4, 5], but a more simple SSJA seems to be not discussed in detail. For random alloys, SSJA correlation factors have been given only for FCC alloys [30]. In this section, we present SSJA correlation factors for both BCC and FCC dilute and random binary alloys using KMFA which for such alloys is exact.

For dilute alloys, we will calculate the tracer correlation factors f_{A^*0} and $f_{B^*0} = f_{B0}$ [2] (where the lower index "0" indicates the $c \to 0$ value for each quantity). For such calculations, we can use Eqs. (30) and (70)–(73) for $c \to 0$ which greatly simplifies these equations. In particular, quantities $\tilde{m}_{B,n}^A$ and $\tilde{A}_{nm}$ in Eqs. (70) and (68) take the following form:

$$\tilde{m}_{B,n,0}^A = -\delta_{n,1}, \qquad \tilde{A}_{nm,0} = 2z_0\delta_{n1}\delta_{m1} + \tilde{t}_{1A,nm,0}^B, \tag{76}$$

where $\tilde{t}^B_{1A,nm,0}$ are given by Eqs. (97)–(100) with replacing each ν_ξ by $e_{A\xi} = e^B_{A\xi}$.

Considering tracer self-diffusion correlation factor f_{A^*0}, we note that all kinetic and saddle-point interactions in the alloy $AB = AA^*$ are absent as atoms A and A^* are chemically identical. Hence, all factors $\eta_{p\xi} = e_{p\xi}$ in Eqs. (58)–(60) are unity, matrices $\tilde{A}_{nm,0}$ in (76) become simple numerical matrices, and "solute" correlation factors $f_{B0} = f_{A^*0}$ in Eqs. (30) and (71)–(73) can be simply evaluated. For completeness, we present SSJA values $f^{\rm SSJA}_{A^*0}$ for both BCC and FCC alloys, together with the NNJA and exact values, $f^{\rm NNJA}_{A^*0}$ and $f^{ex}_{A^*0}$ (given, e. g., in Refs. [2, 24]):

BCC alloys:

$$f^{\rm NNJA}_{A^*0} = \frac{7}{9} = 0.78,$$

$$f^{\rm SSJA}_{A^*0} = \frac{3085}{4179} = 0.7382, \quad f^{ex}_{A^*0} = 0.7272; \tag{77}$$

FCC alloys:

$$f^{\rm NNJA}_{A^*0} = \frac{9}{11} = 0.82,$$

$$f^{\rm SSJA}_{A^*0} = \frac{33247}{41891} = 0.7937, \quad f^{ex}_{A^*0} = 0.7815\,.$$

Equations (77) show, in particular, that the error in f_{A^*0} due to neglecting more distant vacancy-atom correlations for the NNJA and SSJA amounts about 7 % and 1.52 % in BCC alloys, and about 5 % and 1.56 % in FCC alloys, respectively. Hence, SSJA can describe the pairwise vacancy-atom correlations rather accurately.

Let us now discuss the solute correlation factor $f_{B0} = f_{B^*0}$ for dilute alloys. According to Eqs. (30) and (71), it can be written as

$$f_{B0} = 1 - 2z_0 K_{BB,0}, \tag{78}$$

where $K_{BB,0}$ is the $c \to 0$ limit of term K_{BB} in Eq. (72).

To get qualitative ideas about the influence of various kinetic and saddle-point interactions on Onsager coefficients and on correlation factors, below we present explicit expressions for the correlative Onsager coefficients (defined by the general relations (27)) in dilute alloys, $(L^c_{pq})_{c\to 0} = L^{c0}_{pq}$, using the more simple NNJA and the three-neighbor interaction model described by Eqs. (37) and (39). Using Eqs. (74) and (60)–(62), for this model in the NNJA we obtain

BCC alloys:

$$\begin{aligned}
&L^{c0}_{AA} = \frac{2}{D_0} e_1^2 (e_2\zeta_{1A} - e_3\zeta_{2A} - \zeta_{3A})^2,\\
&L^{c0}_{AB} = \frac{2}{D_0} e_1 (e_3\zeta_{2A} + \zeta_{3A} - e_2\zeta_{1A}),\\
&L^{c0}_{BB} = \frac{2z_0}{D_0},\\
&D_0 = e_1(3e_2\zeta_{1A} + 3e_3\zeta_{2A} + \zeta_{3A}) + 2z_0;
\end{aligned} \tag{79}$$

FCC alloys:

$$\begin{aligned}
&L^{c0}_{AA} = \frac{2}{D_0} e_1^2 (2e_1\zeta_{1A} - 2e_2\zeta_{2A} - 1)^2,\\
&L^{c0}_{AB} = \frac{2}{D_0} e_1 (2e_2\zeta_{2A} + 1 - 2e_1\zeta_{1A}),\\
&L^{c0}_{BB} = \frac{2z_0}{D_0},\\
&D_0 = e_1(2e_1\zeta_{1A} + 2e_2\zeta_{2A} + 4e_3\zeta_{3A} + 1) + 2z_0,
\end{aligned}$$

where factors e_n, ζ_{nA}, and z_0 are the same as in Eqs. (62) and (69). The solute correlation factor, according to Eq. (30), is $f_{B0} = 1 - 2z_0/D_0$. For the nearest-neighbor interaction models discussed in detail earlier (see, e. g., [2]), factors e_n and Δ_{nA} with $n \geq 2$ are unity and Eqs. (79) turn into the well-known NNJA results for the "four-frequency" model of BCC alloys or the "five-frequency" model of FCC alloys. Equations (79) show, in particular, that the presence of not-nearest kinetic and saddle-point interactions enhances the correlation factor f_{B0} for positive u_n and negative Δ^B_{nA}, and reduces it for negative u_n and positive Δ^B_{nA}.

Now, we discuss diffusion in random alloys. This simple model was discussed by a number of authors [15–17], in particular, to assess accuracy of various theoretical models using comparison with Monte Carlo studies [17]. In Ref. [30], we used Eqs. (63)–(66) to describe tracer diffusion in FCC random alloys for different values of the frequency ratio $z = z_0 = \omega_{B0}/\omega_{A0}$ in Eqs. (69). Here, we present analogous results for the BCC random alloys.

Treatment of BCC and FCC alloys in our approach is fully similar. Hence, for the BCC alloys, we should just replace the matrix $\mathbf{t}_1^{\rm FCC}$ in Eqs. (81)–(93) of Ref. [30] by $\mathbf{t}_1^{\rm BCC}$ and the term $(9 + \xi)$ in Eq. (90) of [30] by a more general expression, $(t_{11,0} + \xi)$, which for BCC alloys is $(7 + \xi)$. The resulting expressions for tracer correlation factors in BCC and FCC random alloys have the same form:

$$f_{A^*}(c) = f_0 \frac{1+\alpha}{1+\alpha(2f_0-1)}, \quad \alpha = c\frac{z-1}{z+1}, \tag{80}$$

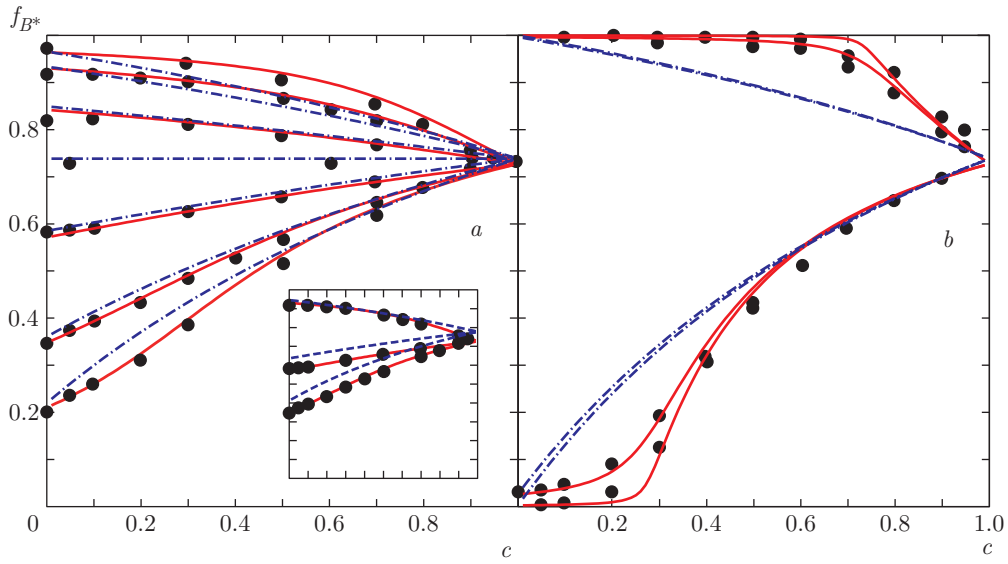

Fig. 6. Tracer correlation factors $f_{B^*}(c)$ for a BCC random alloy found using various methods. Black points show Monte Carlo results [17]; solid curves (red online), Moleko et al. results [16], and dash dotted curves (blue online), SSJA results. Insert in frame (a) shows Monte Carlo, Moleko et al. and NNJA results (dashed curves, purple online). Different groups of points and curves correspond to the following frequency ratios $z = \omega_{B0}/\omega_{A0}$, from top to bottom. Frame (a): 0.1; 0.2; 0.5; 1; 2; 5; 10. Insert in frame (a): 0.2; 2; 5. Frame (b): 0.001; 0.01; 100; 1000

$$f_{B^*}(c,z) = f_{A^*}\left(c_A, \frac{1}{z}\right) = f_0 \frac{1+\beta}{1+\beta(2f_0-1)}, \qquad \beta = c_A \frac{1-z}{1+z}, \tag{81}$$

where f_0 is the correlation factor f_{A^*0} value for the approximation used. For the NNJA, SSJA, and for exact treatments, these values are given in Eqs. (77).

In Fig. 6, we compare correlation factors $f_{B^*}(c)$ for BCC random alloys calculated using SSJA or NNJA with those found in Monte Carlo simulations [17] and in Moleko et al. [16] model which agrees with Monte Carlo simulations almost completely. Correlation factor $f_{A^*}(c)$ can be obtained from these $f_{B^*}(c)$ using the first relation (81). Figure 6 is fully similar to that for FCC random alloys presented in Ref. [30]. At not too different exchange frequencies, $0.2 \lesssim z \lesssim 5$, $f_{B^*}(c)$ found in SSJA or NNJA agree with those found using Monte Carlo and Moleko et al. methods within about 5–10 or 10–20 percents, respectively. At very high (z or $1/z$) $\gtrsim 10^2$, disagreements become large. It points to the importance for such z of non-pairwise vacancy correlation effects (which in the present work are disregarded). This conclusion agrees with that of Ref. [25]. However, for real alloys, frequency ratios z lie usually between about 0.2 and 5, which is illustrated, in particular, by the estimates in Ref. [30] and in Sec. 9 below. For such z, the sufficient accuracy of SSJA and NNJA in description of random alloys shows that the non-pairwise vacancy correlations are not too significant for diffusion. It can also imply that for real alloys, SSJA and NNJA should usually be sufficiently accurate.

8. CONCENTRATION DEPENDENCES OF IRON SELF-DIFFUSION COEFFICIENTS IN BCC ALLOYS Fe–Cu, Fe–Mn, AND Fe–Ni

For BCC alloys FeCu, FeMn, and FeNi, concentration intervals of stability are rather narrow [36]: the solubility limits c_s given in Table 1 are low, and experimental data about concentration dependences of diffusion coefficients within these intervals seem to be absent. At the same time, sharpness of these dependences mentioned in Sec. 5.1 enables us to expect that the variations of diffusion coefficients with concentration c can be noticeable even for these rather narrow intervals $c \lesssim c_s$.

To estimate these variations, we can use the recent *ab initio* calculations of transport coefficients [5] which include calculations of migration barriers for these alloys. For simplicity, we will describe *ab initio* results [5] in terms of our three-neighbor interaction (3NI) models (37) neglecting also the third-neighbor saddle-point interactions: $\Delta^B_{3A} = \Delta^B_{4A} = 0$. As discussed by Messina et al. [5], such models seem to sufficiently accurately

reproduce their results. Then, the results of Ref. [5] for migration barriers in the perfectly ordered ferromagnetic state can be described in terms of kinetic and saddle-point interactions u_n^B, Δ_{1A}^B, and Δ_{2A}^B of the 3NI model (37) which are presented in Table 1.

Table 1. Thermodynamic parameters and interatomic interactions (in eV) in Eqs. (37) which correspond to results of calculations [5] for the four BCC alloys considered

Alloy	T, K	c_s	u_1^B	u_2^B	u_3^B	Δ_{1A}^B	Δ_{2A}^B
FeCu	1000	0.01	0.29	0.13	0.03	0.18	−0.04
FeMn	973	0.02	0.21	0.05	0.05	0.05	0.09
FeNi	973	0.04	0.14	0.11	0.03	0.04	0.09
FeCr	973	0.22	0.08	0	0.02	0.02	0.04

Unfortunately, the fully consistent *ab initio* results have been obtained in [5] only for the perfectly ordered ferromagnetic state. At the same time, diffusion experiments are usually made at high $T \gtrsim 1000$ K when the effects of partial or full magnetic disordering are important. Messina et al. [5] described these effects using some simple model which can be sufficient to treat problems discussed by these authors but seems to be insufficient to describe concentration dependences of diffusion coefficients at $T \gtrsim 1000$ K in which we are interested.

Let us first estimate concentration dependences of iron self-diffusion coefficients $D_{A^*} = D_{\mathrm{Fe}^*}$ for four BCC alloys considered neglecting disordering effects and using "ideal" values of interactions given in Table 1. As solute concentrations $c < c_s$ are very low, concentration dependences in Eq. (32) for D_{A^*} can be taken into account only for the mean frequency ω_A described by Eq. (56):

$$D_{A^*}(c) = D_{A^*0} S_{Aa}^6 S_{Ab}^6 S_{Ac}^2 S_{Ad}^6 S_{Ae}^{18}. \qquad (82)$$

Here, term D_{A^*0} is the self-diffusion coefficient for a pure iron, while factors $S_{p\xi}$ are given by Eqs. (61) and (62). The exponent of each term $S_{p\xi}^{N_\xi} = \exp[N_\xi \ln(1 + c f_{p\xi})]$ in Eq. (82) can be linearized in c. Hence, concentration dependences (82) can be described by a single parameter A_c, to be called the "concentrational increment":

$$D_{A^*}(c) = D_{A^*0} \exp(cA_c), \qquad (83)$$

and this A_c is expressed via the Mayer functions $f_{A\xi} = e_{A\xi} - 1$ in Eqs. (61) as follows:

$$A_c = 6(f_{Aa} + f_{Ab} + f_{Ad}) + 2f_{Ac} + 18 f_{Ae}. \qquad (84)$$

If we use in Eq. (84) values of interactions u_n^B, Δ_{nA}^B, and temperature T given in Table 1, then for alloys FeCu, FeMn, FeNi, and FeCr we obtain increment values (to be referred to as A_c^{id}) equal to 560, 150, 110, and 21, respectively. Such A_c in Eq. (83) would imply that the iron self-diffusion coefficient in alloys FeCu, FeMn, and FeNi increases between $c = 0$ and $c = c_s$ by about 300, 20, and 80 times, respectively. So huge effects could be easily observed and seem to be unrealistic. It seems to indicate that taking into account the above-mentioned magnetic disordering effects is necessary to adequately describe concentration dependences of diffusion coefficients at $T \gtrsim 1000$ K.

To get an idea about the influence of these effects on interactions u_n and Δ_{nA}^B, we can use available experimental data about the concentration dependence of iron self-diffusion coefficients in alloys FeCr [12]. Comparison of these data with the above-mentioned results for "ideal" interactions can enable us to estimate scales and signs of magnetic disordering effects for kinetic and saddle-point interactions.

The results of measurements of $D_{\mathrm{Fe}^*}(c)$ in alloys $\mathrm{Fe}_{1-c}\mathrm{Cr}_c$ for concentrations c between 0 and 0.13 and temperatures T between 933 and 1163 K are described in Ref. [12] by the following relation:

$$D_{\mathrm{Fe}^*}^{\mathrm{FeCr}}(c) = D_{\mathrm{Fe}^*0} \exp[c(4.3T_m/T - 3.2)], \qquad (85)$$

where T_m is the melting temperature being about 1793 K for the concentrations considered [36]. For $T = 973$ K used in Table 1, this relation implies $A_c^{exp} = 4.7$. Comparing this experimental value with the "ideal" $A_c^{id} \approx 21$ mentioned above, we see that magnetic disordering effects lead to a significant reducing of kinetic and saddle-point interactions, by about 5 times, but the sign of A_c in (83) for FeCr alloys at $T \approx 1000$ K still remains positive.

To estimate increments A_c for BCC alloys FeMe with Me=Cu, Mn, or Ni, we can suppose that the scale of this "disordering-induced" reduction of A_c for these alloys is the same as that for alloys FeCr. Then, these increments can be estimated from the "similarity" hypothesis:

$$A_c^{est}(\mathrm{FeMe}) \approx \approx A_c^{id}(\mathrm{FeMe}) \cdot A_c^{exp}(\mathrm{FeCr})/A_c^{id}(\mathrm{FeCr}). \qquad (86)$$

To qualitatively justify this hypothesis, we can consider the case of not too strong kinetic and saddle-point interactions: $u_n^B, \Delta_{nA}^B \lesssim T$ (which is approximately valid for alloys considered at $T \sim 1000$ K). For this case, each Mayer function in Eq. (84), according to Eqs. (37),

(42), and (61), is approximately proportional to interactions u_n^B and Δ_{nA}^B. Then, the "similarity" hypothesis (86) corresponds to the suggestion that the degree of reducing of these interactions due to the magnetic disordering is proportional to the degree of this disordering and is determined only by the ratio of temperature T to the Curie temperature T_c. Such model (analogous to other similar models used to describe effects of magnetic disordering, e. g., that used in Ref. [5]) seems to be reasonable and can be sufficient for the order-of-magnitude estimates made in this section.

Using values $A_c^{id}(\mathrm{FeMe})$, $A_c^{id}(\mathrm{FeCr})$, and $A_c^{exp}(\mathrm{FeCr})$ given above, we estimate values A_c^{est} for alloys FeCu, FeMn, and FeNi to be 130, 34, and 25. It implies that the iron self-diffusion coefficient D_{Fe^*} in these alloys should increase between $c = 0$ and $c = c_s$ by about 3.6, 2, and 2.7 times, respectively. So sharp variations of D_{Fe^*}, by several times within so narrow intervals of concentration, seem to be interesting physical effects which deserve experimental verifications. Measurements of increments A_c in Eq. (83) for alloys FeCu, FeMn, and FeNi can also yield an important information about the real scale of magnetic disordering effects for kinetic and saddle-point interactions for which quantitative theoretical estimates are presently difficult.

9. CONCENTRATION DEPENDENCES OF TRACER AND CHEMICAL DIFFUSION COEFFICIENTS IN BCC ALLOYS IRON-CHROMIUM AT HIGH T

9.1. Features of concentration dependences of diffusion coefficients in alloys FeCr at different temperatures

For BCC alloys FeCr, concentration dependences of both tracer and chemical diffusion coefficients have been studied by many authors [8–14]. Types of these dependences were found to change with elevating temperature T. In particular, the iron self-diffusion coefficient D_{Fe^*} at not high $T \lesssim 1000$ K, according to Eq. (85), does increase with the chromium concentration c, anyway for $c \lesssim 0.2$. On the contrary, at high $T \gtrsim 1400$ K, both tracer and chemical diffusion coefficients sharply decrease with the chromium concentration, as Fig. 7 shows, up to about 4 orders of magnitude, which was noted to be one of the most strong variations of diffusion coefficients with composition known for alloys [10].

Presently, the concentration dependence of each diffusion coefficient D is usually described by the phenomenological "concentration-dependent Arrhenius" model [8–14]:

$$D(c,T) = D_0(c)\exp[-\beta Q(c)], \qquad (87)$$

where $D_0(c)$ and $Q(c)$ is the "frequency factor" and "activation energy", respectively, estimated from data for

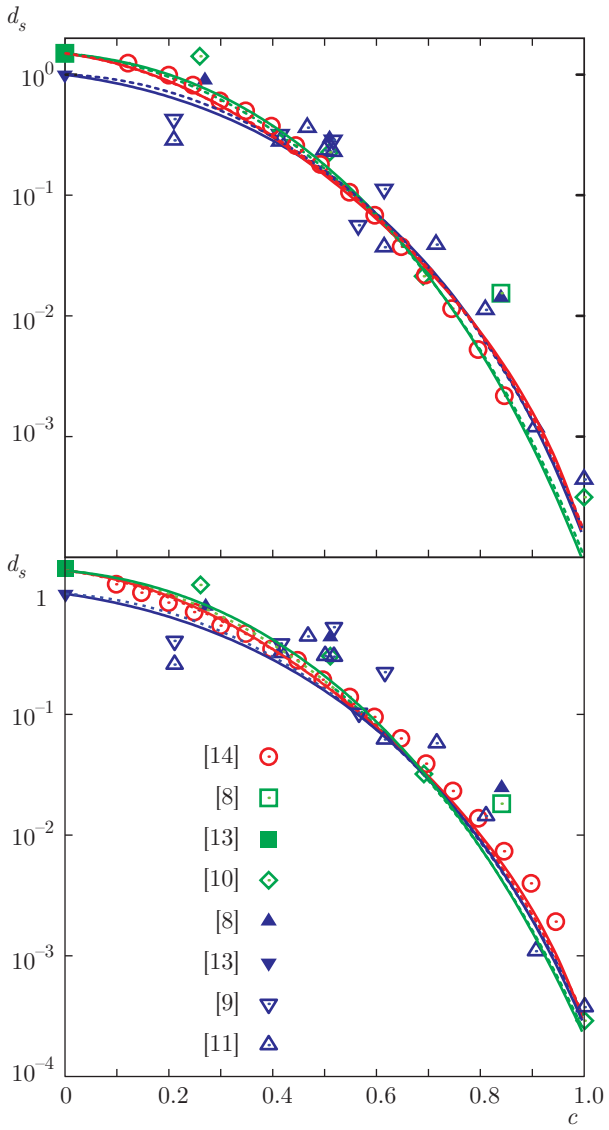

Fig. 7. (Color online) Reduced tracer and chemical diffusion coefficients $d_S(c,T)$ defined by Eqs. (89) for BCC alloys FeCr. The upper frame corresponds to $T = 1473$ K and the lower frame to $T = 1573$ K. Symbols show experimental results taken from sources indicated in the lower frame and curves correspond to calculations. Blue curves and triangles correspond to $d_{\mathrm{Fe}^*}(c,T)$; green curves and squares or rhombi — to $d_{\mathrm{Cr}^*}(c,T)$; red lines and open circles — to $d_{chem}(c,T)$. Dashed or solid curves correspond to the calculations using the parameter set A or B in Table 2

different temperatures and concentrations. Employing model (87) to describe experimental data about tracer diffusion coefficients in alloys FeCr yields anomalous concentration dependences for both functions $D_0(c)$ and $Q(c)$ which have sharp maxima at $c \sim 0.6$, and some exotic models to explain these concentration anomalies have been invoked [10, 11].

However, the phenomenological model (87) has no theoretical justification, and functions $D_0(c)$ and $Q(c)$ used in this model, generally, have no clear physical meaning. Statistical expressions (29) and (32) for diffusion coefficients with the microscopic expressions for mean frequencies and correlation factors discussed in Secs. 3–6 can hardly be described by this model, mainly due to neglecting temperature dependences in the "effective activation energy" $Q(c)$. As discussed in Sec. 5.1, concentration dependences of diffusion coefficients are mainly determined by those of mean frequencies $\omega_p(c)$ given by Eqs. (54)–(56). These equations include Mayer functions $f^{\alpha}_{p\xi} = \exp(\beta\varepsilon^{\alpha}_{p\xi}) - 1$, and temperature dependences of these Mayer functions can be important even when correlation energies $\varepsilon^{\alpha}_{p\xi}$ do not vary with temperature.

At the same time, the magnetic disordering effects mentioned in Sec. 8 seem to lead to a notable decrease of correlation energies $\varepsilon^{\alpha}_{p\xi}$ in alloys FeCr with increasing temperature T. As discussed in Sec. 8, these energies at $T \sim 1000$ K seem to decrease with respect to those for the perfect ordering (corresponding to $T = 0$) by about 5 times, though remain to be mainly positive. It seems natural to suggest that under the further heating to $T \sim 1400$ K and increase of magnetic disordering, these correlation energies go on to decrease, and they change their signs to the mainly negative values. According to Eqs. (54)–(56), it could qualitatively explain the above-mentioned change of types of concentration dependences of iron self-diffusion coefficients in alloys FeCr, from increase to decrease with c, which occurs between $T \sim 1000$ K and $T \sim 1400$ K.

9.2. Physical mechanisms which determine signs of kinetic and saddle-point interactions in alloys FeCr at low and high temperatures

Physical reasons for such changes of types of concentration dependences of diffusion coefficients can be qualitatively understood using microscopic definitions (14) and (4) for kinetic and saddle-point interactions which determine correlation energies $\varepsilon^{\alpha}_{p\xi}$ (for example, by Eqs. (37) for the 3NI model). Let us first discuss kinetic interactions u^{B}_{il} which, according to Table 1 and Eqs. (37), make usually the main contribution to correlation energies. These interactions for alloys FeCr, according to Eq. (14), can be explicitly written as follows:

$$u^{\mathrm{Cr}}_{il} = V^{\mathrm{FeCr}}_{il} - V^{\mathrm{FeFe}}_{il}, \tag{88}$$

where couplings V^{pq}_{il} describe physical interactions in the initial configurational Hamiltonian (1). If we suppose that these couplings in the fully ordered ferromagnetic alloy are mainly determined by magnetic interactions (using for simplicity the "Heisenberg-type" localized spin model), then it is natural to expect that this magnetic coupling between two iron atoms is more negative than that between one iron and a "less magnetic", chromium atom. Hence, kinetic interactions (88) for ferromagnetic alloys with temperatures T much lower than the Curie temperature T_c can be expected to be positive, in agreement with the values presented in Table 1. The analogous considerations can also be used to estimate signs of saddle-point interactions $\Delta^{\mathrm{Cr}l}_{p,ij}$ in Eqs. (4) which are equal to differences in the saddle-point energy $\hat{E}^{SP}$ of a p-species atom due to replacing one of adjacent host atoms Fe by the solute atom Cr. It can qualitatively explain why these saddle-point interactions in Table 1 for alloys FeCr (as well as for FeCu, FeMn, and FeNi) are as a rule positive.

At the same time, at high $T \gtrsim T_c$, magnetic contributions to the total energy sharply decrease, and other, "exchange" effects related to the filling of electronic d-bands by d-electrons in an alloy, can become most important. Qualitatively, these effects are known to be very successfully described by the Friedel tight-binding model [39, 40] which naturally explains the peculiar form of dependences of cohesive energy E_{coh} in transition metals on the number z_d of d-electrons per atom. This tight-binding model considers the filling of "bonding" and "antibonding" d-orbitals between neighboring atoms in a d-metal to make the main contribution to the cohesive energy. Other effects, such as those related to crystal fields, $s - d$ hybridization, etc, are supposed to be of the secondary importance. Then, the cohesive energy $E_{coh}(z_d)$ should reach maximum when all bonding orbitals with both directions of spin are occupied, while all antibonding orbitals are empty, that is, at $z_d = 5$. It agrees well with positions of maxima E^{max}_{coh} for all three rows of transition metals, $3d$, $4d$, and $5d$, observed at $z_d \approx 5$, while variations of $E_{coh}(z_d)$ within each row are quite large being 5–10 eV/atom [39, 40]. Note that these "exchange" arguments neglect magnetic effects as they consider occupations of d-orbitals with both directions of spin to be the main factor in binding.

For two components of iron-chromium alloys, z_d values for chromium and iron atoms are $z^{\mathrm{Cr}}_d = 4$ and $z^{\mathrm{Fe}}_d =$

= 6, respectively. Hence, using the simplest version of Friedel model described above, we can expect that the formation of d-orbitals between an atom Cr and an atom Fe can yield the notable gain in the binding energy with respect to that for two atoms Fe. Then, using again Eq. (88) and the analogous considerations for saddle-point energies, we can expect that the values of both kinetic interactions u_{il}^{Cr} and saddle-point interactions $\Delta_{p,ij}^{\mathrm{Cr}l}$ in alloys FeCr at high T (when the magnetic effects fade out) are mainly negative. This competition between magnetic effects at low $T \ll T_c$ and "exchange" effects at high $T \gtrsim 1400$ K can qualitatively explain changes of signs of kinetic and saddle-point interactions in alloys FeCr with elevating T noted in Sec. 9.1.

9.3. Estimates of kinetic and saddle-point interactions in alloys FeCr for high temperatures

For high $T \gtrsim 1400$ K, experimental data of many authors about both tracer and chemical diffusion coefficients in BCC alloys FeCr are available. Some of these data are presented in Fig. 7. Even though these data have a notable scatter (which can be partly related to the above-mentioned inaccuracies of Eq. (87) in description of data for different temperatures), main features of concentration dependences of diffusion coefficients seem to be described by these data quite definitely. Hence, these data and the theory described in Secs. 3–6 can be used to estimate the kinetic and saddle-point interactions in alloys FeCr for these temperatures. Below, we do it for $T = T_1 = 1473$ K and $T = T_2 = 1573$ K for which detailed data [14] about the chemical diffusion coefficients $D_{chem}(c)$ are available.

For convenience of comparison of theoretical and experimental results for different diffusion coefficients D_S (where symbol S corresponds to Fe^*, Cr^*, or "chem"), below we consider the "reduced" diffusion coefficients $d_S(c,T)$ defined as the ratios of each $D_S(c,T)$ to the iron self-diffusion coefficient $D_{\mathrm{Fe}^*0}(T)$ in a pure iron:

$$\begin{gathered} d_{\mathrm{Fe}}^* = D_{\mathrm{Fe}}^*/D_{\mathrm{Fe}^*0}, \quad d_{\mathrm{Cr}}^* = D_{\mathrm{Cr}}^*/D_{\mathrm{Fe}^*0}, \\ d_{chem} = D_{chem}/D_{\mathrm{Fe}^*0}. \end{gathered} \tag{89}$$

Experimental values D_{Fe^*0} will be taken from Ref. [13] for the paramagnetic α iron:

$$\begin{gathered} D_{\mathrm{Fe}^*0} = D_0 \exp\left(-\beta Q_{\mathrm{Fe}^*}\right), \\ D_0 = 1.77 \text{ cm}^2/\text{s}, \quad Q_{\mathrm{Fe}^*} = 236.5 \text{ kJ/mol}. \end{gathered} \tag{90}$$

Note that the D_{Fe^*0} values given by Eqs. (90) for $T = T_1$ and $T = T_2$ (used in Fig. 7) do practically coincide with those obtained using the earlier interpolation [38]; it can confirm the reliability of these values.

Theoretical expressions for reduced diffusion coefficients $d_S(c)$ (89) can be obtained using general equations (31) and (32). These equations include the "dilatation factor" $a_0^2(c)/a_0^2(0) = (1+c\nu)^{2/3}$, where $\nu = \bar{v}_B/\bar{v}_A - 1$ with $\bar{v}_B$ and $\bar{v}_A$ from Eq. (28) is the dilatation parameter. For alloys FeCr, this parameter is very low, $\nu \approx 0.02$, and can be neglected. Hence, the reduced diffusion coefficients (89) can be written as follows:

$$\begin{gathered} d_{A^*} = \frac{\omega_A}{\omega_{A0}} \frac{f_{A^*}}{f_{A^*0}}, \quad d_{B^*} = \frac{\omega_B}{\omega_{A0}} \frac{f_{B^*}}{f_{A^*0}}, \\ d_{chem} = \left(c_A \frac{\omega_B}{\omega_{A0}} \frac{f_B}{f_{A^*0}} + c \frac{\omega_A}{\omega_{A0}} \frac{f_A}{f_{A^*0}} \right) \Phi, \end{gathered} \tag{91}$$

where we use for brevity symbol A for Fe and symbol B for Cr. Putting in these equations $c \to 0$ and denoting values $(d_S)_{c\to 0}$ as d_{S0}, we obtain following relations for the low-c values of reduced diffusion coefficients:

$$\begin{gathered} d_{A^*0} = 1, \quad d_{B^*0} = z_0 f_{B0}/f_{A^*0}, \\ d_{chem,0} = d_{B^*0}. \end{gathered} \tag{92}$$

Here, z_0, f_{A^*0}, and $f_{B0} = f_{B^*0}$ are the same as in Eqs. (69), (77), and (78). Note that for the temperatures T considered, the BCC alloys FeCr are stable only at not too low $c \gtrsim 0.12$ [36], and relations (92) hold actually for extrapolated values. At the same time, a good accuracy of the third relation (92) for extrapolated experimental values $(d_{chem})_{c\to 0}$ and d_{B^*0} in Fig. 7 seems to confirm the reliability of these different extrapolations.

For the thermodynamic factor Φ and the activity coefficient a_B (defined, e. g., by Eqs. (107)–(112) in Ref. [29]) which enter Eqs. (91) and (56), we use the available CALPHAD data for BCC alloys FeCr [37] omitting magnetic contributions (being negligible at high T considered). It yields

$$\begin{gathered} \Phi = 1 + c c_A \varphi_T, \quad \varphi_T = 2.33 - 4930/T[\mathrm{K}], \\ a_B = \exp(c\varphi_T). \end{gathered} \tag{93}$$

These data show, in particular, that the thermodynamic interactions $v^{BB} = v^{\mathrm{CrCr}}$ in BCC alloys FeCr are rather weak. For example, using the PCA expression (53), we find for the Mayer function corresponding to the nearest-neighbor interaction $f_1^{BB} \approx -\varphi_T/8 \sim 0.1$. Such weak interactions also imply that the fluctuation effects (discussed in Sec. 6) here are insignificant for statistical averages; it is also illustrated by Fig. 3. Hence, the simple KMFA described in Sec. 5 is sufficient to quantitatively evaluate these averages.

Table 2. Parameters of 2NI and 3NI models for BCC alloys FeCr used in the calculations shown in Fig. 7

Set	$z_0(T_1)$	Interactions, eV										
		u_1^B	u_2^B	u_3^B	Δ_{1A}^B	Δ_{1B}^B	Δ_{2A}^B	Δ_{2B}^B	Δ_{3A}^B	Δ_{3B}^B	Δ_{4A}^B	Δ_{4B}^B
A	1.78	0.0389	−0.2132	0	−0.0948	−0.0821	−0.0584	−0.0681	0	0	0	0
B	1.89	0.0469	−0.1833	0.0152	−0.0931	0.0644	0.0311	−0.0386	−0.0308	0.0950	0.0658	−0.0682

In our estimates of kinetic and saddle-point interactions, we will use two models: the three-neighbor interaction (3NI) model described by Eqs. (37) and the two-neighbor interaction (2NI) model which corresponds to putting in Eqs. (37) $u_3^B = \Delta_{3p}^B = \Delta_{4p}^B = 0$. The 3NI model includes 11 interaction parameters presented in Table 2, and the 2NI model, 6 interaction parameters. In addition to that, we should also estimate the frequency ratio z_0 in Eqs. (92). We will suppose that between $T = 1473$ K and $T = 1573$ K there are no significant variations in both interaction constants and in activation energies Q_{Fe^*} and Q_{Cr^*} for tracer diffusion in a pure iron. Then, using data [13] for these activation energies, we find that the frequency ratios z_0 at T_1 and T_2 are related as

$$z_0(T_2) = 1.08\, z_0(T_1). \tag{94}$$

Hence, mathematically, our problem is reduced to the estimate of 12 (for 3NI models) or 7 (for 2NI models) unknown parameters from six experimental curves for $d_S(c, T_1)$ and $d_S(c, T_2)$ presented in Fig. 7.

Taking also into account the notable scatter of experimental data presented in Fig. 7, it is evident that such estimates can not be very definite, particularly for 3NI models. However, our estimates aim mainly at not quantitative but qualitative tasks discussed below.

As fluctuation effects for alloys considered seem to be negligible, the reduced diffusion coefficients d_S in Eqs. (91) were calculated using the SSJA-KMFA expressions for mean frequencies and correlation factors given in Sec. 5. For the chosen interaction model, 2NI or 3NI one, the parameter set $\{x_n\} = \{u_n^B, \Delta_{pn}^B, z_0\}$ (limited by constraints discussed below) was found from the condition of the best fit of six calculated curves $d_S(c, T_1)$ and $d_S(c, T_2)$ to experimental points shown in Fig. 7, that is, the condition of the absolute minimum of the sum of deviations $\Sigma\{x_n\}$ (sum of moduli of differences between experimental and calculated values of d_S) for the parameter set $\{x_n\}$:

$$\Sigma\{x_n\} = \Sigma_{min},$$

$$\Sigma\{x_n\} = \sum_{S,c_i} \sum_{T=T_1}^{T_2} |(d_S(c_i, T) - d_S(c_i, T)^{exp}|\,, \tag{95}$$

where c_i are concentrations for which diffusion coefficients $d_S(c_i, T)$ have been measured.

In seeking parameter sets $\{x_n\}$ minimizing the sum of deviations (95), we took into account the following physical considerations. (i) Values of kinetic interactions $|u_n^B|$ for the two nearest neighbors, $n = 1$ and $n = 2$, are expected to notably exceed the more distant ones: $|u_3^B| < |u_{1,2}^B|$ (which is illustrated, in particular, by the *ab intitio* estimates [5] presented in Table 1). Although *ab initio* information on the saddle point interactions for the 3rd and 4th neighbors is not available, it would be reasonable to expect that the saddle point interactions for these more distant neighbors do not exceed considirably those for the 1st and 2nd neighbors. (ii) In accordance with physical considerations discussed in Sec. 9.2, we expect that at least one of significant kinetic interactions, u_1^B or u_2^B, is negative. (iii) Maximum values of saddle-point interactions $|\Delta_{np}^B|_{max}$, generally, are expected to be lower than the maximum values of kinetic interactions $|u_n^B|_{max}$ (which is again illustrated by Table 1).

In accordance with considerations (i)–(iii), we put various constraints on the parameter sets $\{x_n\}$ minimizing the sum of deviations (95). At the same time, we found that the resulting values $\{x_n\}$ are not very sensitive to the particular form of these constraints. In Table 2, we present two typical sets of parameters $\{x_n\}$, labeled as A and B, which correspond to the following constraints used (in eV):

$$\begin{aligned} &A\colon\ 2NI \text{ model; } |u_{1,2}^B| < 0.3, \quad |\Delta_{1p,2p}^B| < 0.15; \\ &B\colon\ 3NI \text{ model; } |u_{1,2}^B| < 0.3, \quad |u_3^B| < 0.1, \\ &\qquad\qquad |\Delta_{1p,2p}^B| < 0.15, \quad |\Delta_{3p,4p}^B| < 0.1. \end{aligned} \tag{96}$$

In Fig. 7, we show the fit of experimental data obtained using parameter sets A and B presented in Table 2. The figure shows that the quality of the fit is practically the same for both these sets (as well as for other similar sets). Hence, such fits enable us to estimate the parameter sets $\{x_n\}$ only within their scatter illustrated by Fig. 7. At the same time, the results presented in Fig. 7 and Table 2 enable us to make following qualitative conclusions.

1. First, we see that the very strong and peculiar concentration dependences of diffusion coefficients observed in these alloys can be naturally explained by

the present statistical theory, without invoking various exotic models discussed earlier [10, 11].

2. Second, we see that in spite of significant quantitative uncertainties, our analysis enables us to make some qualitative conclusions about the signs and the scales of kinetic and saddle-point interactions in alloys considered. Our experience of using most different forms of constraints for parameter sets $\{x_n\}$ in Eq. (95) (illustrated by Eqs. (96)) have shown that the reasonable fit of experiments in Fig. 7 can be obtained only if at least one of kinetic interactions, u_1^B or u_2^B, takes a significant negative value. It agrees with the probable importance of exchange effects in alloys considered discussed in Sec. 9.2. For the sets presented in Table 2, the second constant u_2^B takes such significant negative value. However, elucidation of relations between u_1^B or u_2^B, in particular, that of importance of spin correlations between first and second neighbors in alloys considered, can need more detailed *ab initio* treatments. At the same time, signs of saddle-point interactions Δ_{np}^B estimated in Table 2 are negative for the 2NI model, in a qualitative agreement with considerations discussed in Sec. 9.2.

10. CONCLUSION

In this paper, we are presenting the further major development of statistical theory of diffusion in concentrated alloys. With the amendments made to the theory it is now possible to take into account interatomic interactions of atoms located at lattice sites with arbitrary distance between them. Thus, the developed theory can be used for precision calculations of both chemical and tracer diffusion coefficients in real alloys with arbitrary interatomic interactions.

To validate the theory, we applied it to BCC alloys FeCu, FeMn, FeNi, and FeCr. For alloys FeCu, FeMn, and FeNi the solubility limit is very low: $c_s \lesssim \lesssim (0.01\text{–}0.04)$. We predict sharp increase in iron self diffusion coefficient up to 2–4 times as solute concentration spans this narrow range. These results imply that using methods designed specifically to treat dilute alloys may lead to notable inaccuracies in this case.

For FeCr alloys at high temperatures above 1400 K, we made calculations of chemical and tracer diffusion coefficients and compared our results with the available experimental data. At such temperatures solubility range for FeCr alloys is very broad varying between 0.12 and 1.0 Cr content and values of diffusion coefficients fall by the factor of 10^4 with increase of Cr concentration. Strong concentration dependences of diffusion coefficients are naturally explaned by the theory without using any phenomenological considerations, and results of calculation are in good agreement with the experiment.

Physical mechanisms which determine signs and magnitude of kinetic and saddle point interactions for FeCr alloys at high temperatures are disscussed. Values of kinetic and saddle point interactions are estimated and used in calculations of diffusion coefficients.

Quality of analytical statistical approximations: Pair Cluster Approximation (PCA) used for calculations of site chemical potentials and Kinetic Mean Field Approximation (KMFA) used for calculations of jump frequencies and correlation factors is checked by analyzing the same properties using Metropolis Monte Carlo algorithm. It is found that these approximate statistical methods have rather high quality at arbitrary concentrations.

The work was supported in part by the Russian Fund of Basic Research (grants Nos. 12-02-00093 and 15-02-02084-a), and by the State Task FANO (theme "Spin", no. g/r 01201463330). The results of the work were obtained using computational resources of MCC NRC "Kurchatov Institute" (http://computing.kiae.ru/).

APPENDIX 1

Symmetries and positions of lattice sites considered in this work for BCC and FCC alloys

Table A1. Changes of positions of lattice sites under turns of the BCC lattice which transform bonds $(0, k)$ shown in Fig. 1 into bond (0,1)

k	Components of vector $\mathbf{R}$	Position of sites							
1	(x, y, z)	1	2	3	4	5	6	7	8
2	$(-y, x, z)$	4	1	2	3	8	5	6	7
3	$(-x, -y, z)$	3	4	1	2	7	8	5	6
4	$(y, -x, z)$	2	3	4	1	6	7	8	5
5	$(y, -z, x)$	2	3	7	6	1	4	8	5
6	$(-z, -y, x)$	3	4	8	7	2	1	5	6
7	$(-z, -x, -y)$	7	3	4	8	6	2	1	5
8	$(-z, y, -x)$	8	7	3	4	5	6	2	1

Table A2. The same as in Table A1 but for the FCC lattice shown in Fig. 2

k	Components of vector $\mathbf{R}$	Position of sites											
1	(x,y,z)	1	2	3	4	5	6	7	8	9	10	11	12
2	$(-y,x,z)$	4	1	2	3	8	5	6	7	12	9	10	11
3	$(-x,-y,z)$	3	4	1	2	7	8	5	6	11	12	9	10
4	$(y,-x,z)$	2	3	4	1	6	7	8	5	10	11	12	9
5	$(x,-z,y)$	3	10	7	11	1	9	5	12	2	6	8	4
6	$(-y,-z,x)$	11	3	10	7	12	1	9	5	4	2	6	8
7	$(x,-y,-z)$	7	6	5	8	3	2	1	4	10	9	12	11
8	$(y,-z,-x)$	10	7	11	3	9	5	12	1	6	8	4	2
9	$(-z,y,x)$	12	4	11	8	9	2	10	6	1	3	7	5
10	$(-z,x,-y)$	8	12	4	11	6	9	2	10	5	1	3	7
11	$(z,-x,-y)$	6	10	2	9	8	11	4	12	7	3	1	5
12	$(z,y,-x)$	9	6	10	2	12	8	11	4	5	7	3	1

Table A3. Geometrical characteristics of sites i_ξ with different symmetries ξ in Eq. (33) for a BCC alloy

ξ	j	a	b	c	d	e_1	e_2	f_1	f_2	f_3	f_4	f_5	f_6
m,n	0,1	1,2	1,3	1,5	2,4	3,4	3,7	4,5	4,6	4,8	4,9	5,7	5,10
$N(i_\xi)$	2	6	6	2	6	12	6	12	6	12	6	6	2

Table A4. The same as in Table A3 but for an FCC alloy

ξ	j	a	b	c	d	e	f	g	h_1	h_2	h_3	h_4	i_1	i_2	i_3
m,n	0,1	1,1	1,2	1,3	1,4	2,3	2,5	3,3	3,4	3,5	3,6	3,7	4,5	4,7	4,9
$N(i_\xi)$	2	4	4	8	2	4	4	4	8	8	4	8	4	8	2

Table A5. Positions $\mathbf{R}_i$ and symmetries ξ of sites i in BCC alloys

i	0	1	2	3	4	5	6	7	8	$\bar{1}$	$\bar{2}$	$\bar{3}$	$\bar{4}$	$\bar{5}$	$\bar{6}$	$\bar{7}=0$	$\bar{8}$
$\mathbf{R}_i$	000	111	$1\bar{1}1$	$\bar{1}\bar{1}1$	$\bar{1}11$	$11\bar{1}$	$1\bar{1}\bar{1}$	$\bar{1}\bar{1}\bar{1}$	$\bar{1}1\bar{1}$	222	202	002	022	220	200	000	020
ξ	j	j	a	b	a	a	b	c	b	c	b	a	b	b	a	j	a

i	$a_1=\bar{3}$	$a_2=\bar{8}$	$a_3=\bar{6}$	a_4	a_5	a_6	$\bar{a}_1$	$\bar{a}_2$	$\bar{a}_3$	$\bar{a}_4=5$	$\bar{a}_5=2$	$\bar{a}_6=4$
$\mathbf{R}_i$	002	020	200	$00\bar{2}$	$0\bar{2}0$	$\bar{2}00$	113	131	311	$11\bar{1}$	$1\bar{1}1$	$\bar{1}11$
ξ	a	a	a	d	d	d	d	d	d	a	a	a

i	$b_1=\bar{4}$	b_2	$b_3=\bar{2}$	b_4	b_5	b_6	b_7	b_8	$b_9=\bar{5}$	b_{10}	b_{11}	b_{12}
$\mathbf{R}_i$	022	$0\bar{2}2$	202	$\bar{2}02$	$02\bar{2}$	$0\bar{2}\bar{2}$	$20\bar{2}$	$\bar{2}0\bar{2}$	220	$\bar{2}20$	$\bar{2}\bar{2}0$	$2\bar{2}0$
ξ	b	e_1	b	e_1	e_1	e_2	e_1	e_2	b	e_1	e_2	e_1

i	$\bar{b}_1$	$\bar{b}_2$	$\bar{b}_3$	$\bar{b}_4$	$\bar{b}_5$	$\bar{b}_6=6$	$\bar{b}_7$	$\bar{b}_8=8$	$\bar{b}_9$	$\bar{b}_{10}$	$\bar{b}_{11}=3$	$\bar{b}_{12}$
$\mathbf{R}_i$	133	$1\bar{1}3$	313	$\bar{1}13$	$13\bar{1}$	$1\bar{1}\bar{1}$	$31\bar{1}$	$\bar{1}1\bar{1}$	331	$\bar{1}31$	$\bar{1}\bar{1}1$	$3\bar{1}1$
ξ	e_2	e_1	e_2	e_1	e_1	b	e_1	b	e_2	e_1	b	e_1

i	$c_1=\bar{a}_2$	$c_2=\bar{a}_3$	$c_3=\bar{b}_{12}$	c_4	c_5	c_6	c_7	$c_8=\bar{b}_{10}$	$c_9=\bar{b}_5$	$c_{10}=\bar{b}_7$	c_{11}	c_{12}	c_{13}	c_{14}	c_{15}	c_{16}
$\mathbf{R}_i$	131	311	$3\bar{1}1$	$1\bar{3}1$	$\bar{1}\bar{3}1$	$\bar{3}\bar{1}1$	$\bar{3}11$	$\bar{1}31$	$13\bar{1}$	$31\bar{1}$	$3\bar{1}\bar{1}$	$1\bar{3}\bar{1}$	$\bar{1}\bar{3}\bar{1}$	$\bar{3}\bar{1}\bar{1}$	$\bar{3}1\bar{1}$	$\bar{1}3\bar{1}$
ξ	d	d	e_1	f_2	f_3	f_3	f_2	e_1	e_1	e_1	f_1	f_3	f_4	f_4	f_3	f_1

i	$\bar{c}_1$	$\bar{c}_2$	$\bar{c}_3$	$\bar{c}_4$	$\bar{c}_5=b_2$	$\bar{c}_6=b_4$	$\bar{c}_7$	$\bar{c}_8$	$\bar{c}_9$	$\bar{c}_{10}$	$\bar{c}_{11}$	$\bar{c}_{12}=b_{12}$	$\bar{c}_{13}=a_5$	$\bar{c}_{14}=a_6$	$\bar{c}_{15}=b_{10}$	$\bar{c}_{16}$
$\mathbf{R}_i$	242	422	402	$2\bar{2}2$	$0\bar{2}2$	$\bar{2}02$	$\bar{2}22$	042	240	420	400	$2\bar{2}0$	$0\bar{2}0$	$\bar{2}00$	$\bar{2}20$	040
ξ	f_4	f_4	f_3	f_1	e_1	e_1	f_1	f_3	f_3	f_3	f_2	e_1	d	d	e_1	f_2

i	$d_1=\bar{a}_1$	$d_2=\bar{b}_4$	d_3	$d_4=\bar{b}_2$	d_5	d_6	d_7	d_8	$\bar{d}_1$	$\bar{d}_2$	$\bar{d}_3$	$\bar{d}_4$	$\bar{d}_5$	$\bar{d}_6=b_5$	$\bar{d}_7=a_4$	$\bar{d}_8=b_7$
$\mathbf{R}_i$	113	$\bar{1}13$	$\bar{1}\bar{1}3$	$1\bar{1}3$	$11\bar{3}$	$\bar{1}1\bar{3}$	$\bar{1}\bar{1}\bar{3}$	$1\bar{1}\bar{3}$	224	024	004	204	$22\bar{2}$	$02\bar{2}$	$00\bar{2}$	$20\bar{2}$
ξ	d	e_1	f_1	e_1	f_2	f_3	f_4	f_3	f_4	f_3	f_2	f_3	f_1	e_1	d	e_1

i	$g_1=\bar{1}$	g_2	g_3	g_4	g_5	g_6	g_7	g_8	$\bar{g}_1$	$\bar{g}_2$	$\bar{g}_3=d_3$	$\bar{g}_4$	$\bar{g}_5$	$\bar{g}_6=c_{11}$	$\bar{g}_7=7$	$\bar{g}_8=c_{16}$
$\mathbf{R}_i$	222	$2\bar{2}2$	$\bar{2}\bar{2}2$	$\bar{2}22$	$22\bar{2}$	$2\bar{2}\bar{2}$	$\bar{2}\bar{2}\bar{2}$	$\bar{2}2\bar{2}$	333	$3\bar{1}3$	$\bar{1}\bar{1}3$	$\bar{1}33$	$33\bar{1}$	$3\bar{1}\bar{1}$	$\bar{1}\bar{1}\bar{1}$	$\bar{1}3\bar{1}$
ξ	c	f_1	f_5	f_1	f_1	f_5	f_6	f_5	f_6	f_5	f_1	f_5	f_5	f_1	c	f_1

APPENDIX 2

Expressions for terms $t^q_{1p,nm}$ in Eq. (24) via one-site averages

In this section, we express terms $t^q_{1p,nm}$ in Eq. (24) via one-site averages $\nu^q_{p\xi}$ used in Eqs. (45). For brevity, below in this section we omit the common lower index p and the common upper index q at $\nu^q_{p\xi}$ writing it as simply ν_ξ.

For BCC alloys, terms $t^q_{1p,nm}$ are elements of the following matrix:

$$\mathbf{t}^q_{1p} = \begin{pmatrix} t_{11} & -\nu_a & -2\nu_b & 0 & 0 & -\nu_c \\ -4\nu_a & t_{22} & 0 & 0 & -4\nu_d & 0 \\ -2\nu_b & 0 & t_{33} & -2\nu_{e_1} & -2\nu_{e_1} & 0 \\ 0 & 0 & -\nu_{e_1} & t_{44} & 0 & -\nu_{f_1} \\ 0 & -\nu_d & -2\nu_{e_1} & 0 & t_{55} & -\nu_{f_1} \\ -\nu_c & 0 & 0 & -2\nu_{f_1} & -\nu_{f_1} & t_{66} \end{pmatrix}, \quad (97)$$

where the diagonal elements t_{nn} are

$$\begin{aligned} &t_{11}=3\nu_a+3\nu_b+\nu_c, \quad t_{22}=4(\nu_a+\nu_d),\\ &t_{33}=2(\nu_b+2\nu_{e_1}+\nu_{e_2}), \quad t_{44}=t_{55},\\ &t_{55}=\nu_d+2\nu_{e_1}+\nu_{f_1}+\nu_{f_2}+2\nu_{f_3}+\nu_{f_4},\\ &t_{66}=\nu_c+3\nu_{f_1}+3\nu_{f_5}+\nu_{f_6}. \end{aligned} \quad (98)$$

For FCC alloys, matrix $t^q_{1p,nm}$ in Eq. (24) has the following form:

$$\mathbf{t}^q_{1p} = \begin{pmatrix} t_{11} & -\nu_b & -2\nu_c & -2\nu_c & -\nu_d \\ -4\nu_b & t_{22} & 0 & -4\nu_e & 0 \\ -\nu_c & 0 & t_{33} & -\nu_g & -\nu_{h_1} \\ -2\nu_c & -\nu_e & -2\nu_g & t_{44} & -2\nu_{h_1} \\ -\nu_d & 0 & -2\nu_{h_1} & -2\nu_{h_1} & t_{55} \end{pmatrix}, \quad (99)$$

where the diagonal elements t_{nn} are

$$\begin{aligned} &t_{11}=2\nu_a+2\nu_b+4\nu_c+\nu_d, \quad t_{22}=4(\nu_b+\nu_c+\nu_f),\\ &t_{33}=2\nu_c+\nu_e+\nu_g+2\nu_{h_1}+2\nu_{h_2}+\nu_{h_3}+2\nu_{h_4},\\ &t_{44}=t_{33}+\nu_g,\\ &t_{55}=\nu_d+4\nu_{h_1}+2\nu_{i_1}+4\nu_{i_2}+\nu_{i_3}. \end{aligned} \quad (100)$$

APPENDIX 3

Expressions for reduced coefficients $\tilde{t}^{q\lambda}_{2p,nm}$ in Eqs. (57) in the kinetic mean-field approximation

In this section, we use the following shortened notation for the product of factors $\eta^q_{p\xi}$ and $\eta^\lambda_{p\xi}$ defined by Eq. (59):

$$\xi\xi' = \eta^q_{p\xi}\eta^\lambda_{p\xi}. \quad (101)$$

Table A6. The same as in Table A5 but for FCC alloys

i	0	1	2	3	4	5	6	7	8	9	10	11	12
$\mathbf{R}_i$	000	011	101	$0\bar{1}1$	$\bar{1}01$	$01\bar{1}$	$10\bar{1}$	$0\bar{1}\bar{1}$	$\bar{1}0\bar{1}$	110	$1\bar{1}0$	$\bar{1}\bar{1}0$	$\bar{1}10$
ξ	j	j	a	b	a	b	c	d	c	a	c	c	a

i	$\bar{1}$	$\bar{2}$	$\bar{3}$	$\bar{4}$	$\bar{5}$	$\bar{6}=9$	$\bar{7}=0$	$\bar{8}=12$	$\bar{9}$	$\bar{1}0=2$	$\bar{1}\bar{1}=4$	$\bar{1}\bar{2}$
$\mathbf{R}_i$	022	112	002	$\bar{1}12$	020	110	000	$\bar{1}10$	121	101	$\bar{1}01$	$\bar{1}21$
ξ	d	c	b	c	b	a	j	a	c	a	a	c

i	$a_1=\bar{3}$	$a_2=\bar{5}$	a_3	a_4	a_5	a_6	$\bar{a}_1$	$\bar{a}_2$	$\bar{a}_3$	$\bar{a}_4=5$	$\bar{a}_5=3$	$\bar{a}_6$
$\mathbf{R}_i$	002	020	200	$0\bar{2}0$	$00\bar{2}$	$\bar{2}00$	013	031	211	$01\bar{1}$	$0\bar{1}1$	$\bar{2}11$
ξ	b	b	e	f	f	e	f	f	e	b	b	e

i	$b_1=\bar{9}$	$b_2=\bar{5}$	b_3	b_4	b_5	b_6	b_7	$b_8=\bar{1}\bar{2}$	b_9	b_{10}	b_{11}	b_{12}	b_{13}	b_{14}	b_{15}	b_{16}
$\mathbf{R}_i$	121	211	$2\bar{1}1$	$1\bar{2}1$	$\bar{1}\bar{2}1$	$\bar{2}\bar{1}1$	$\bar{2}11$	$\bar{1}21$	$12\bar{1}$	$21\bar{1}$	$2\bar{1}\bar{1}$	$1\bar{2}\bar{1}$	$\bar{1}\bar{2}\bar{1}$	$\bar{2}\bar{1}\bar{1}$	$\bar{2}1\bar{1}$	$\bar{1}2\bar{1}$
ξ	c	e	h_1	h_2	h_2	h_1	e	c	g	h_1	h_3	h_4	h_4	h_3	h_1	g

i	$\bar{b}_1$	$\bar{b}_2$	$\bar{b}_3$	$\bar{b}_4$	$\bar{b}_5$	$\bar{b}_6$	$\bar{b}_7$	$\bar{b}_8=a_3$	$\bar{b}_9=10$	$\bar{b}_{10}=11$	$\bar{b}_{11}$	$\bar{b}_{12}$	$\bar{b}_{13}$	$\bar{b}_{14}$	$\bar{b}_{15}$	$\bar{b}_{16}$
$\mathbf{R}_i$	132	222	202	$1\bar{1}2$	$\bar{1}\bar{1}2$	$\bar{2}02$	$\bar{2}22$	$\bar{1}32$	130	220	200	$1\bar{1}0$	$\bar{1}\bar{1}0$	$\bar{2}00$	$\bar{2}20$	$\bar{1}30$
ξ	h_4	h_3	h_1	g	g	h_1	h_3	h_4	h_2	h_1	e	c	c	e	h_1	h_2

i	$c_1=\bar{2}$	$c_2=\bar{4}$	$c_3=\bar{b}_5$	$c_4=\bar{b}_4$	c_5	c_6	c_7	c_8	$\bar{c}_1$	$\bar{c}_2$	$\bar{c}_3$	$\bar{c}_4$	$\bar{c}_5=b_9$	$\bar{c}_6=b_{16}$	$\bar{c}_7=8$	$\bar{c}_8=6$
$\mathbf{R}_i$	112	$\bar{1}12$	$\bar{1}\bar{1}2$	$1\bar{1}2$	$11\bar{2}$	$\bar{1}1\bar{2}$	$\bar{1}\bar{1}\bar{2}$	$1\bar{1}\bar{2}$	123	$\bar{1}23$	$\bar{1}03$	103	$12\bar{1}$	$\bar{1}2\bar{1}$	$10\bar{1}$	$10\bar{1}$
ξ	c	c	g	g	h_2	h_2	h_4	h_4	h_4	h_4	h_2	h_2	g	g	c	c

i	$d_1=\bar{1}$	$d_2=\bar{b}_3$	d_3	$d_4=\bar{b}_6$	d_5	d_6	d_7	d_8	d_9	d_{10}	d_{11}	$d_{12}=\bar{b}_{15}$
$\mathbf{R}_i$	022	202	$0\bar{2}2$	$\bar{2}02$	$02\bar{2}$	$20\bar{2}$	$0\bar{2}\bar{2}$	$\bar{2}0\bar{2}$	220	$2\bar{2}0$	$\bar{2}\bar{2}0$	$\bar{2}20$
ξ	d	h_1	i_1	h_1	i_1	i_2	i_3	i_2	h_1	i_2	i_2	h_1

i	$\bar{d}_1$	$\bar{d}_2$	$\bar{d}_3$	$\bar{d}_4$	$\bar{d}_5$	$\bar{d}_6=b_{10}$	$\bar{d}_7=7$	$\bar{d}_8=b_{15}$	$\bar{d}_9$	$\bar{d}_{10}=b_9$	$\bar{d}_{11}=b_6$	$\bar{d}_{12}$
$\mathbf{R}_i$	033	213	$0\bar{1}3$	$\bar{2}13$	$03\bar{1}$	$21\bar{1}$	$0\bar{1}\bar{1}$	$\bar{2}1\bar{1}$	231	$2\bar{1}1$	$\bar{2}\bar{1}1$	$\bar{2}\bar{3}1$
ξ	i_3	i_2	i_1	i_2	i_1	h_1	d	h_1	i_2	h_1	h_1	i_2

Then, each $\tilde{t}^{q\lambda}_{2p,nm}$ in (57) for BCC or FCC alloys can be written as the sum of two terms:

$$\tilde{t}^{q\lambda}_{2p,nm} = A_n B_m \gamma_n \gamma_m + \tau^{q\lambda}_{nm}. \qquad (102)$$

Here, A_n and B_m are numerical constants given in Table A7, while γ_n are the following linear combinations of symbols of symmetry ξ in Tables A1 or A2:

Table A7. Values of numerical factors A_n and B_m in Eq. (102)

Alloy	A_1	A_2	A_3	A_4	A_5	A_6	B_1	B_2	B_3	B_4	B_5	B_6
BCC	1	4	2	1	1	1	2	2	4	4	2	2
FCC	1	4	1	2	1		2	2	4	4	2	

BCC :

$$\begin{aligned}
&\gamma_1 = a - b - c, \quad \gamma_2 = a - d,\\
&\gamma_3 = b - e_2, \quad \gamma_4 = d - f_1 + f_2 - f_4,\\
&\gamma_5 = d + 2e_1 + f_1 - f_2 - 2f_3 - f_4,\\
&\gamma_6 = c + f_1 - f_5 - f_6;
\end{aligned} \qquad (103)$$

FCC:

$$\begin{aligned}
&\gamma_1 = 2a - 2c - d, \quad \gamma_2 = b - f,\\
&\gamma_3 = c + e - g + h_2 - h_3 - h_4,\\
&\gamma_4 = c + g - h_2 - h_4,\\
&\gamma_5 = d + 2h_1 - 2i_2 - i_3.
\end{aligned}$$

In the notation (101), matrix $\hat{\tau}^{q\lambda}$ in (102) for BCC alloys can be written as follows:

$$\hat{\tau}^{q\lambda} = \begin{pmatrix} \tau_{11} & aa & 2bb & 0 & 0 & cc \\ 4aa & \tau_{22} & 0 & 0 & 4dd & 0 \\ 2bb & 0 & \tau_{33} & 2e_1e_1 & 2e_1e_1 & 0 \\ 0 & 0 & e_1e_1 & \tau_{44} & 0 & f_1f_1 \\ 0 & dd & 2e_1e_1 & 0 & \tau_{55} & f_1f_1 \\ cc & 0 & 0 & 2f_1f_1 & f_1f_1 & \tau_{66} \end{pmatrix},$$

where the diagonal elements τ_{nn} are

$$\begin{aligned} &\tau_{11} = -(3aa + 3bb + cc), \quad \tau_{22} = -4(aa + dd), \\ &\tau_{33} = -(2bb + 4e_1e_1 + 2e_2e_1), \quad \tau_{44} = \tau_{55}, \\ &\tau_{55} = -(dd + 2e_2e_1 + f_1f_1 + f_2f_2 + 2f_3f_3 + f_4f_4), \\ &\tau_{66} = -(cc + 3f_1f_1 + 3f_5f_5 + f_6f_6). \end{aligned} \tag{104}$$

For FCC alloys, the analogous relations have the form

$$\hat{\tau}^{q\lambda} = \begin{pmatrix} \tau_{11} & bb & 2cc & 2cc & dd \\ 4bb & \tau_{22} & 0 & 4ee & 0 \\ cc & 0 & \tau_{33} & gg & h_1h_1 \\ 2cc & ee & 2gg & \tau_{44} & 2h_1h_1 \\ dd & 0 & 2h_1h_1 & 2h_1h_1 & \tau_{55} \end{pmatrix}$$

with the following diagonal elements τ_{nn}:

$$\begin{aligned} &\tau_{11} = -(2aa + 2bb + 4cc + dd), \\ &\tau_{22} = -4(bb + cc + ff), \quad \tau_{33} = \tau_{44} + gg, \\ &\tau_{44} = -(2cc + ee + 2gg + 2h_1h_1 + 2h_2h_2 + \\ &\qquad + h_3h_3 + 2h_4h_4), \\ &\tau_{55} = -(dd + 4h_1h_1 + 2i_1i_1 + 4i_2i_2 + i_3i_3). \end{aligned} \tag{105}$$

REFERENCES

1. J.-L. Bocquet, Acta Metall. **20**, 1347 (1974).

2. A. R. Alnatt and A. B. Lidiard, *Atomic Transport in Solids*, Cambridge Univ. Press, Cambridge (1993).

3. S. Chooudhury, L. Barnard, J. D. Tucker, T. R. Allen, B. D. Wirth, M. Asta, and D. Morgan, J. Nucl. Mater. **411**, 1 (2011).

4. T. Garnier, M. Nastar, P. Bellon, and D. R. Trinkle, Phys. Rev. B **88**, 134201 (2013).

5. L. Messina, M. Nastar, T. Garnier, C. Domain, and P. Olsson, Phys. Rev. B **90**, 104203 (2014).

6. N. S. Kulkarni, PhD Dissertation, Univ. of Florida (2004).

7. I. V. Belova, N. S. Kulkarni, Y. H. Sohn, and G. E. Murch, Phil. Mag. **93**, 3515 (2013).

8. L. I. Ivanov and N. P. Ivanchev, Izvest. Akad. Nauk, Otdel. Tekhn. Nauk, August (1958), p. 15.

9. A. Ya. Shinyaev, All-Union Conference on the Use of Isotopes and Nuclear Radiations, Moscow (1958), p. 299.

10. H. W. Paxton and T. Kunitake, Trans AIME **218**, 1003 (1960).

11. A. Ya. Shinyaev, Fiz. Met. Metallovedenie **20**, 875 (1965).

12. J. Kucera, B. Million, J. Ruzickova, V. Foldyna, and A. Jakobova, Acta. Met. **22**, 135 (1974).

13. J. Kucera and K. Stransky, Mater. Sci. Eng. **52**, 1 (1982).

14. V. V. Popov, Defect and Diffusion Forum **283–286**, 687 (2009).

15. J. R. Manning, Phys. Rev. B **4**, 1111 (1971).

16. L. K. Moleko, A. R. Allnatt, and E. L. Allnatt, Phil. Mag. A **59**, 141 (1989).

17. I. V. Belova and G. E. Murch, Phil. Mag. A **80**, 1409 (2000).

18. N. A. Stolwijk, Phys. Stat. Sol. (b) **105**, 223 (1981).

19. I. V. Belova and G. E. Murch, Defect and Diffusion Forum **143–147**, 309 (1997).

20. H. Sato and R. Kikuchi, Phys. Rev. B **28**, 648 (1982).

21. S. A. Akbar, J. Mater. Sci. **27**, 3125 (1992).

22. C. C. Wang and S. A. Akbar, Acta Metall. Mater. **41**, 2807 (1993).

23. K. D. Belashchenko and V. G. Vaks, J. Phys.: Condensed Matter **10**, 1965 (1998).

24. M. Nastar, V. Yu. Dobretsov, and G. Martin, Phil. Mag. A **80**, 155 (2000).

25. V. Barbe and M. Nastar, Phil. Mag. **86**, 1513 (2006).

26. M. Nastar and V. Barbe, Faraday Discussions **134**, 331 (2007).

27. M. Nastar, Phil. Mag. **85**, 3767 (2005).

28. V. G. Vaks and I. A. Zhuravlev, JETP **115**, 634 (2012).

29. V. G. Vaks, A. Yu. Stroev, I. R. Pankratov, and A. D. Zabolotskiy, JETP **119**, 272 (2014).

30. V. G. Vaks, A. Yu. Stroev, I. R. Pankratov, K. Yu. Khromov, A. D. Zabolotskiy, and I. A. Zhuravlev, Phil. Mag. **95**, 1536 (2015).

31. F. Soisson and C.-C. Fu, Phys. Rev. B **76**, 214102 (2007).

32. F. Soisson, C. Becquart, N. Castin, C. Domain, L. Malerba, and E. Vincent, J. Nucl. Mater. **406**, 55 (2010).

33. D. P. Landau and K. Binder, *A Guide to Monte Carlo Simulations in Statistical Physics*, Cambridge Univ. Press, Cambridge (2009).

34. V. G. Vaks and G. D. Samolyuk, JETP **88**, 89 (1999).

35. V. G. Vaks, F. Soisson, and I. A. Zhuravlev, Phil. Mag. **93**, 3084 (2013).

36. Alloy Phase Diagrams, ASM Handbook, Vol. 3 (1992).

37. J.-O. Andersson, Metall. Trans. A **19**, 627 (1988).

38. D. Graham and D. H. Tomlin, Phil. Mag. **8**, 1581 (1963).

39. J. Friedel, in: *The Physics of Metals*, Vol. 1: *Electrons*, ed. by J. M. Ziman, Cambridge Univ. Press, Cambridge (2011).

40. V. G. Vaks, *Interatomic Interactions and Binding in Solids*, IzdAT, Moscow (2002), Ch. 12.5 (in Russian).